Ore Geology Reviews 89 (2017) 290–308

Contents lists available at ScienceDirect

Ore Geology Reviews

journal homepage: www.elsevier.com/locate/oregeo

Comparison between Datangpo-type manganese ores and modern marine ferromanganese oxyhydroxide precipitates based on rare earth elements

JiaFei Xiao [a,*], JingYang He [b], HaiYing Yang [a,c], Chengquan Wu [a,c]

[a] State Key Laboratory of Ore Deposit Geochemistry, Institute of Geochemistry, Chinese Academy of Science, Guiyang, 550081 Guiyang, China
[b] School of Earth Sciences and Resources, China University of Geosciences, Beijing, Haidian, 100083 Beijing, China
[c] University of Chinese Academy of Sciences, Beijing, Haidian, 100049 Beijing, China

ARTICLE INFO

Article history:
Received 30 May 2016
Received in revised form 8 June 2017
Accepted 12 June 2017
Available online 23 June 2017

Keywords:
Manganese deposits
Marine ferromanganese precipitates
Deposit genesis
REE geochemistry

ABSTRACT

Datangpo-type sedimentary manganese deposits, which are located in northeastern Guizhou province and its adjacent areas, are Mn carbonate-type deposits hosted in black carbonaceous shale that represent a series of medium to large deposits containing a huge tonnage of reserves. PAAS-normalized rare earth element distribution patterns of manganese ores record "hat-shaped" REY (REE + Y) plots characterized by pronounced middle rare earth element enrichment, evident positive Ce anomalies, weak to strong positive Eu anomalies and negligible negative Y anomalies. These REY geochemical characteristics are different from those of country rocks and record the processes and features of sedimentation and diagenesis. Manganese was precipitated as Mn-oxyhydroxide particles in oxidized water columns with the sorption of a certain amount of rare earth elements, subsequently transforming from Mn-oxyhydroxides to rhodochrosite and redistributing REY in reducing alkaline pore-water during early diagenesis. A number of similarities can be observed through a comparison of Datangpo-type manganese ores and modern marine ferromanganese oxyhydroxide precipitates based on their rare earth elements. The precipitation of Datangpo-type manganese ores is similar to that of hydrogenetic crusts and nodules based on their positive Ce anomalies and relatively higher total REY concentrations. However, several differences also exist. Compared to hydrogenetic crusts and nodules, Datangpo-type manganese ores record smaller positive Ce anomalies, lower total REY concentrations, unobvious fractionation between Y and Ho, and weak to strong positive Eu anomalies. These were caused by quicker sedimentary rates in the oxic water columns of the shallower basin, after which pore water became strongly reducing and alkaline due to the degradation of organic matter in the early diagenetic stage. In addition, compared to typical deposits in the world, Datangpo-type manganese ores are similar to hydrogenetic deposits and different than hydrothermal deposits. All of these characteristics of manganese ores indicate that Datangpo-type manganese ores, the principal metallogenic factors of which include oxidation conditions during deposition and reducing conditions during early diagenetic stages, represent hydrogenetic deposits.

1. Introduction

Marine sedimentary manganese deposits formed during the Nanhuan (equivalent to the Cryogenian) Period, which are among the most important manganese ore resources in China (Fan and Yang, 1999; Hou et al., 1997), are mainly located in the northeastern region of Guizhou province, the mid-western region of Hunan province, the southeastern region of Chongqing City and Changyang county of Hubei province. In northeastern Guizhou province and its adjacent regions, manganese deposits are commonly referred to as "Datangpo-type" manganese deposits, as they are mainly found in the Nanhuan Datangpo Formation and are hosted in black carbonaceous shale as manganese carbonates (e.g., rhodochrosite, calico-rhodochrosite). Thus far, a series of medium- to large-scale manganese deposits of economic significance (e.g., Yanglizhang, Dawu, Datangpo, Daotuo, Xixibao, Minle, Rongxi, and Gucheng) (Fig. 1) have been explored and developed, as they exhibit high levels of prospecting potential.

However, the genesis of the Datangpo-type manganese deposits remains controversial due to complex processes of metallogenesis. Since the 1980s, a series of contrasting genetic theories have been

* Corresponding author.
E-mail address: xiaojiafei@vip.gyig.ac.cn (J. Xiao).

http://dx.doi.org/10.1016/j.oregeorev.2017.06.016
0169-1368/

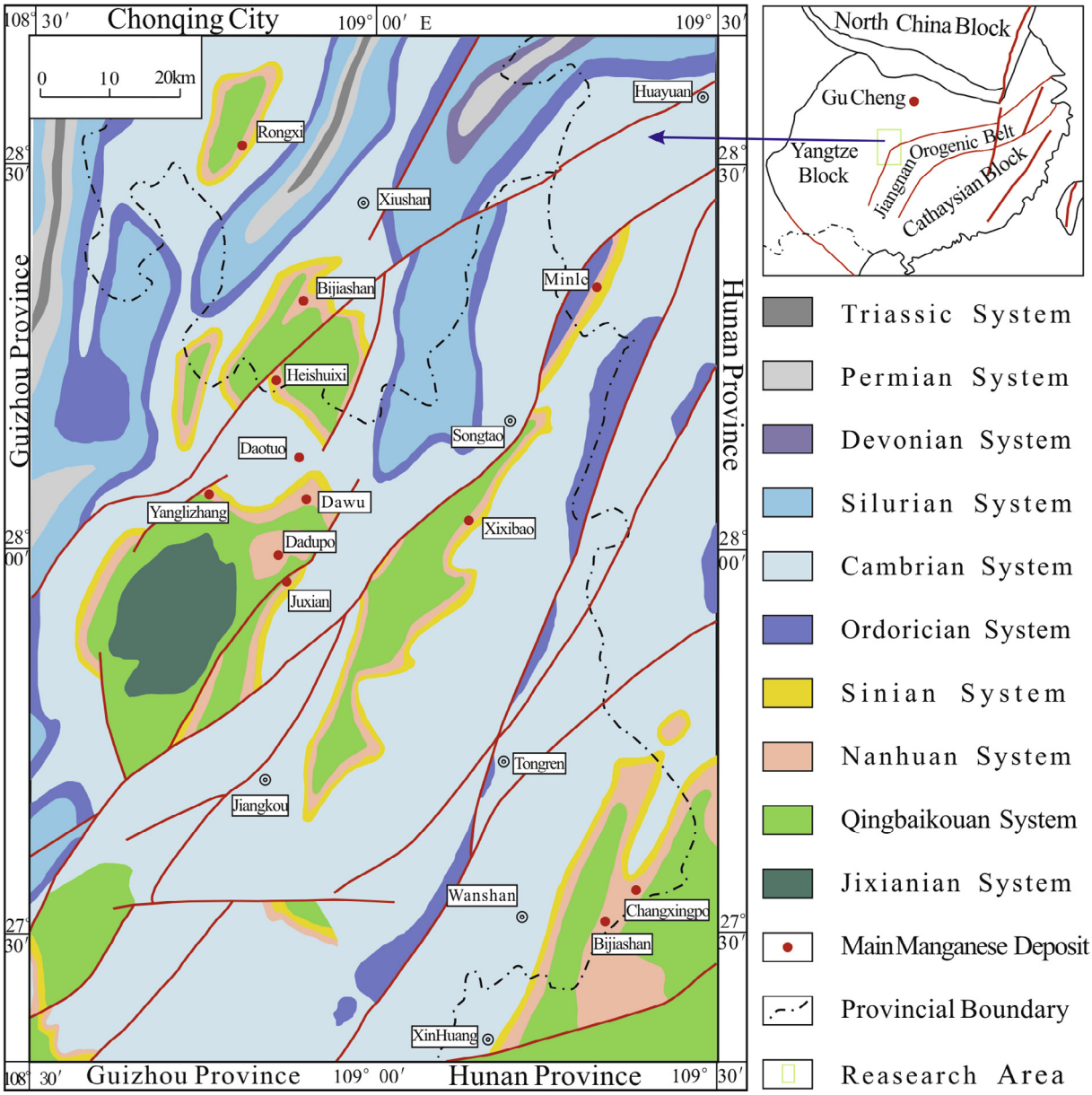

Fig. 1. Schematic geological map of northeastern Guizhou and It's adjacent areas and the distribution of main Cryogenian manganese ore deposits (tectonic location was modified based on Shu, 2012; geological sketch map was modified based on Geological map of Guizhou Province, 1987; Geological map of Hunan Province, 1988; Geological map of Sichuan Province, 1990).

proposed, including biogenic origins (Liu et al., 1983, 1989; Zheng and Liu, 1987), hydrothermal origins (Wang, 1990), gravity flow deposits (Zhao, 1990), multi-source biology-turbidity deposits (Liu, 1994), cap carbonate deposits (Yang et al., 2002), volcanic eruption and precipitation (Yang and Lao, 2006), and cold seep carbonate deposits (Zhou et al., 2013,; Zhou et al., 2007a,b), among others. Most of these theories have concluded that manganese is directly precipitated as manganese carbonate in reductive water columns. Nevertheless, in recent years, some scholars have argued that manganese is precipitated as insoluble Mn-oxyhydroxide particles in oxidized water columns, which are then transformed into rhodochrosite through bacterial sulfate reduction in alkaline anoxic interstitial water below the oxidation-reduction interface early in the diagenetic process (An et al., 2014; Zhang et al., 2013a,b,c; Zhu et al., 2013). This theory reflects the genetic processes of most marine sedimentary manganese carbonate deposits and manganese-bearing sediments found around the world (e.g., Calvert and Pedersen, 1996; Chisonga et al., 2012; Nyame et al., 2003; Okita et al., 1988; Okita and Shanks III, 1992; Polgári et al., 2012; Roy, 2006; Sabatino et al., 2011).

If Datangpo-type manganese ores are precipitated as oxyhydroxides under oxic conditions and are then transformed to rhodochrosite through organic carbon-mediated changes during initial diagenetic processes, do the geochemical characteristics of manganese ores emerge during the sedimentary-diagenetic process? In particular, are there similarities between Datangpo-type manganese ores and marine ferromanganese oxyhydroxide precipitates? If so, what are their associated similarities and differences? In addition, modern marine ferromanganese oxyhydroxide deposits with significant levels of manganese metallogenesis have been identified, which have attracted considerable attention and led to systematic achievements in studies of mineralogy, geochemistry, formation environments, growth processes and genetic classifications due to their considerable

economic resource potential (e.g., Bau et al., 2014; Canet et al., 2008; Roy, 1992; Surya Prakash et al., 2012; Takematsu et al., 1989; Usui and Terashima, 1997). These ferromanganese precipitates are of vital metallogenic significance to the study of manganese deposits that have developed throughout geological history. Although some scholars have made comparisons between Datangpo-type manganese ores and marine ferromanganese oxyhydroxide precipitates, these comparisons only prove either that manganese ore is precipitated under oxic conditions, based on similarities in their REE distribution patterns (An et al., 2014; Zhu et al., 2013), or that hydrothermal activities can influence these deposits, based on the results of Fe-Mn-(Cu + Ni + Co) × 10 ternary plots (e.g., Tan et al., 2009; Wang, 1990). One remaining question concerns whether these comparisons are correct and reasonable if analyses regarding their similarities and differences are not integrated. In addition, variations between these differences, and their causes, require further discussion.

In order to identify the metallogenetic process of the Datangpo-type manganese ores, this paper analyses the geochemical characteristics of manganese ores collected from different mining areas using rare earth element data and examines the different genetic types of marine ferromanganese precipitates by examining the similarities and differences between Datangpo-type manganese ores and marine ferromanganese oxyhydroxide precipitates through a comparison of their mineralization mechanisms. To our knowledge, this is the first detailed comparison that has been made between Datangpo-type manganese deposits and marine ferromanganese oxyhydroxide precipitates. The results of this comparative analysis will further our knowledge of the genesis of Datangpo-type manganese deposits. Furthermore, metallogenic mechanism and metallogenic type of Datangpo-type manganese ores can be ulteriorly explained by comparing to REE geochemistry of the country rocks as well as typical manganese deposits around the world.

2. Geological setting

In the study area, mainly Sinian-Silurian strata and minor Devonian and Permian-Triassic strata are exposed. Folds and fractures are NE-trending. The manganese-bearing rock series, which is distributed in the wing of an anticline (Fig. 1), has an irregular lenticular shape in profile, with a width of 500–3000 m, a length of 5000–7000 m and a NE-trending long axis. Datangpo-type manganese deposits are mainly found in the border areas of Guizhou province, Hunan province and Chongqing City (Fig. 1). Consequently, they are found in what is referred to as the "Guizhou-Hunan-Chongqing" Manganese Triangle in China. This area includes a complex fold belt with a basement of Mesoproterozoic and Neoproterozoic low-grade metamorphic rocks located within the Yangtze Block and the Jiangnan orogenic belt (Fig. 1). The area has undergone multiple phases of intense tectonic activity, including the amalgamation of the Yangtze and Cathaysia Blocks, which formed the South China Block in the late Mesoproterozoic, and the subsequent inner breakup and amalgamation events that occurred in the South China Block (Dai et al., 2010; Liu et al., 1993).

The Mid-Neoproterozoic lithostratigraphy perfectly records the tectonic evolution of the research area (Table 1). The Wuling orogeny (1.0–0.9 Ga, Li et al., 2009; Ye et al., 2007; also referred to as the Sibao or Jinning orogeny in the literature), which is represented by an angular unconformity at the bottom of the Neoproterozoic stratum (Dai et al., 2010, Table 1), caused the first amalgamation of the Yangtze and Cathaysia Blocks. Then, the regional tectonic evolution entered a new stage: the Xuefeng-Caledonian tectonic cycle. As the rifting and fragmentation of the supercontinent Rodinia occurred in the early Neoproterozoic, the Yangtze and Cathaysia Blocks began to break up once again, producing the Neoproterozoic Nanhua rift systems no later than 820 Ma (Wang et al., 2001,2006). Under these conditions, a series

Table 1
Lithostratigraphy and tectonic evolution during the Mesoproterozoic and Neoproterozoic in northeastern Guizhou and adjacent areas in China (achieved synthetically based on Dai et al., 2010; Dobrzinski and Bahlburg, 2007; Lin et al., 2013; Lu et al., 2010; Wang et al., 2001).

<table>
<tr><th colspan="3">Stratigraphic Unit / Rgion</th><th>Northeastern of Guizhou and adjacent region</th><th>Southeastern of Guizhou and Northern of Guangxi</th><th>Sedimentary Formation</th><th>Tectonic Stage</th><th>Tectonic Cycle</th></tr>
<tr><td colspan="3">Period/System</td><td colspan="2">Cambrian Period/System</td><td rowspan="2">Carbonate -Shale- Silicolite Formation</td><td rowspan="6">Passive Margin</td><td rowspan="8">Xuefeng-Caledonian Tectonic Cycle</td></tr>
<tr><td rowspan="8">Neoproterozoic</td><td rowspan="2">Sinian</td><td></td><td>Dengying FM.</td><td>Laobao FM.</td></tr>
<tr><td colspan="2">Doushantuo FM.</td></tr>
<tr><td rowspan="5">Nanhuaan</td><td>Nantuo Glaciation</td><td>Nantuo FM.</td><td>Lijiapo FM.</td><td>Lijiapo FM.</td><td rowspan="4">Moraine Clastic Formation</td></tr>
<tr><td>Fulu Inter-glaciation</td><td>Chengjiang FM.</td><td>Datangpo FM.
Tiesi'ao FM.
Liangjiehe FM.</td><td>Datangpo FM.
Fulu FM.</td></tr>
<tr><td>Chang'an Glaciation</td><td>Gap</td><td></td><td>Changan FM.</td></tr>
<tr><td>Xuefeng Movement</td><td colspan="3"></td></tr>
<tr><td colspan="2">Qingbaikou</td><td>Banxi Group</td><td>Xiajiang Group / Danzhou Group</td><td>Molasse and Flysch Formation</td><td>Rift Basin</td></tr>
<tr><td colspan="3">Wuling Movement</td><td colspan="2"></td><td></td><td></td><td></td></tr>
<tr><td>Meso-proterozoic</td><td colspan="2">Jingxian-Changcheng</td><td>Fanjingshan Group</td><td>Sibao Group / Sibao Group</td><td></td><td></td><td>Wuling Tectonic Cycle</td></tr>
</table>

of graben-horst sub-basins progressively developed in the southeastern margin of the Yangtze Block (e.g., the Xiang-Gui sub-basin, located in the research area, which provided enough space for Neoproterozoic sedimentation to occur) (Jiang et al., 2003; Wang et al., 2001). Thereafter, the southeastern margin of the Yangtze Block progressively evolved into a passive continental margin during the Xuefeng orogeny (Wang et al., 2012; Table 1), which was characterized by more stable platform deposition, including moraine clastic formation during the Nanhua Period and carbonate-shale-silicalite formation during the Sinian and Cambrian Periods (Table 1).

Meanwhile, Neoproterozoic Cryogenian global glaciations resulted in at least two glacial deposits and one interglacial deposit in the Nanhuan sedimentary sequence located along the southeastern margins of the Yangtze Block. The first glacial period (the Chang'an glaciation) developed a moraine, referred to as the Chang'an Formation, which absented sedimentation in the northeastern margin of the Xiang-Gui sub-basin by covering the continental glacier. The second glacial period (the Nantuo glaciation) formed the Nantuo and Lijiapo Formations, which comprise continental glacial and marine glacial deposits, respectively, in the Xiang-Gui sub-basin. During the interglacial period, the Fulu Formation, Datangpo Formation and corresponding strata developed through transient transgression after the Chang'an glaciation (Liu et al., 1993; Lu et al., 2010; Wang et al., 2001; Ye et al., 2007; Yin et al., 2006, and references therein). Several studies have shown that the Chang'an and Nantuo glaciations are equivalent to the Sturtian (c. 720 Ma) and Marinoan (c. 600–635 Ma) glaciations of the Cryogenian Period, respectively (e.g., Dobrzinski and Bahlburg, 2007; Yin et al., 2006; Zhou et al., 2004).

The Datangpo stage, which occurred during the interglacial period in intertropical and subtropical climates featuring the appearance and proliferation of algae, is characterized by carbon-bearing,

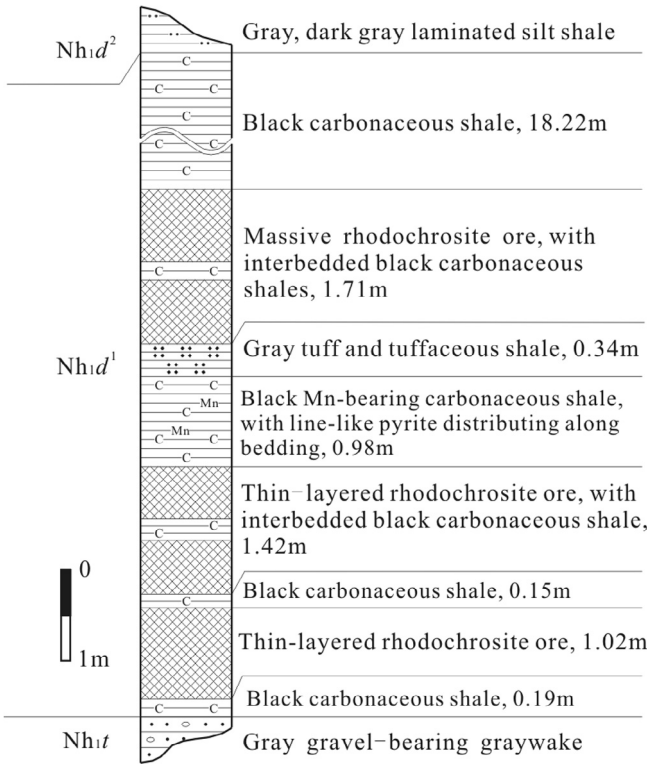

Fig. 2. Stratigraphic column of the first member of Datangpo Formation at ZK001 of the Daotuo manganese ore deposit (Qin et al., 2013). Nh_1d^1 and Nh_1d^2 denote the first and second members of Datangpo Formations, respectively, and Nh_1t denotes the Tiesi'ao Formation.

fine-grained deposition in an epicontinental semi-limited shallow basin surrounded by barrier islands, due to the uneven settlement of the basin basement. The Datangpo Formation underlies the Nantuo and/or Lijiapo Formations and overlies the Tiesi'ao and/or Fulu Formations (the Tiesi'ao Formation is believed to be equivalent to the upper Fulu Formation, according to Lin et al., 2013; Lu et al., 2010). Furthermore, the Datangpo Formation is usually divided into two members, based on its lithologic characteristics (Fig. 2). The first member, or the black carbonaceous shale member, ranges from 2 to 50 m and includes black carbonaceous shale, black manganese-bearing carbonaceous shale, lenticular dolomite, high contents of star-like pyrite and organic matter, and distinct horizontal bedding. This member is usually referred to as the "manganese-bearing rock series," as its main stratigraphic horizon includes economically significant manganese deposits. The second member, which ranges from 30 to 320 m, mainly includes gray and dark gray silty mudstone and mudstone with negligible carbon matter with a distinct laminated structure (Lin et al., 2013; Qin et al., 2005). The U-Pb zircon ages obtained from volcanic tuff samples from the basal Datangpo Formation are 662.9 ± 4.3 Ma (Zhou et al., 2004), 667.3 ± 9.9 Ma (Yin et al., 2006), and 661 ± 7 Ma (Gao et al., 2013), while the U-Pb zircon age of an ash bed at the summit of the Datangpo Formation (0.6 m below the Nantuo glacial diamictite) is 654.5 ± 3.8 Ma (Zhang et al., 2008). These U-Pb zircon ages roughly define the minimum and maximum ages of the Datangpo Formation.

Manganese deposits are distributed in a dispersive and directional manner; deposits are located several kilometers to tens of kilometers apart from each other and exhibit NE-trending distribution.

Datangpo-type manganese deposits, which are largely hosted in the black carbonaceous shale of the first member of Datangpo Formation (Fig. 2), are usually composed of 1–3 layers of manganese ore beds. The morphologies of the ore bodies mainly include lenticular (Fig. 3A) and quasi-lamellar (Fig. 3B) structures. Lenticular ore bodies are distributed in the lower to middle part of the manganese-bearing series, which contain concentrated orebody groups consisting of different sizes of lenticular structures, which are arranged and combined in fish-like, en-echelon, oblique and jagged shapes. Quasi-lamellar ore bodies, which extend further and are more stable, contain 1–3 layers of carbonaceous shale (Wang et al., 1985). Rhodochrosite is mainly hosted in the thicker sections of the manganese-bearing rock series with a maximum thickness of approximately 10–50 m. The content of organic carbon in the carbonaceous shale distributed in the ore-concentrated area is 2–3% (Liu et al., 1989). In the first member of Datangpo Formation, the total thicknesses of the ore beds vary and tend to increase with increasing thickness. Hence, the thickest ore bed is usually located in the center of the basin; this thickness diminishes from the center of the basin to its margins, thus showing an obvious control over strata (Xie et al., 2014).

Massive (Fig. 3C, D) and banded ores (Fig. 3E, F) are the two main ore types. The former has sparse, discontinuous and inconspicuous lamina, whereas the latter has dense and conspicuous lamina.

The sedimentary characteristics of manganese ore are as follows: it is melanocratic (mainly black and black gray) and has a micritic texture with granular and biological structures. This micritic texture is characterized by interlayered, 0.03-mm-long rhodochrosite crystals. The particles forming the granular texture are sand-sized grains, blocky masses, pellets, biodetritus (e.g., fucoid, algal clastic), and minor terrigenous detrital grains and tephra. The characteristics of the sedimentary structures are mainly massive bedding (Fig. 3C, D) with undeveloped lamina, banded bedding (Fig. 3E, F) constituted by interphase black rhodochrosite bands and gray argillaceous bands, and horizontal

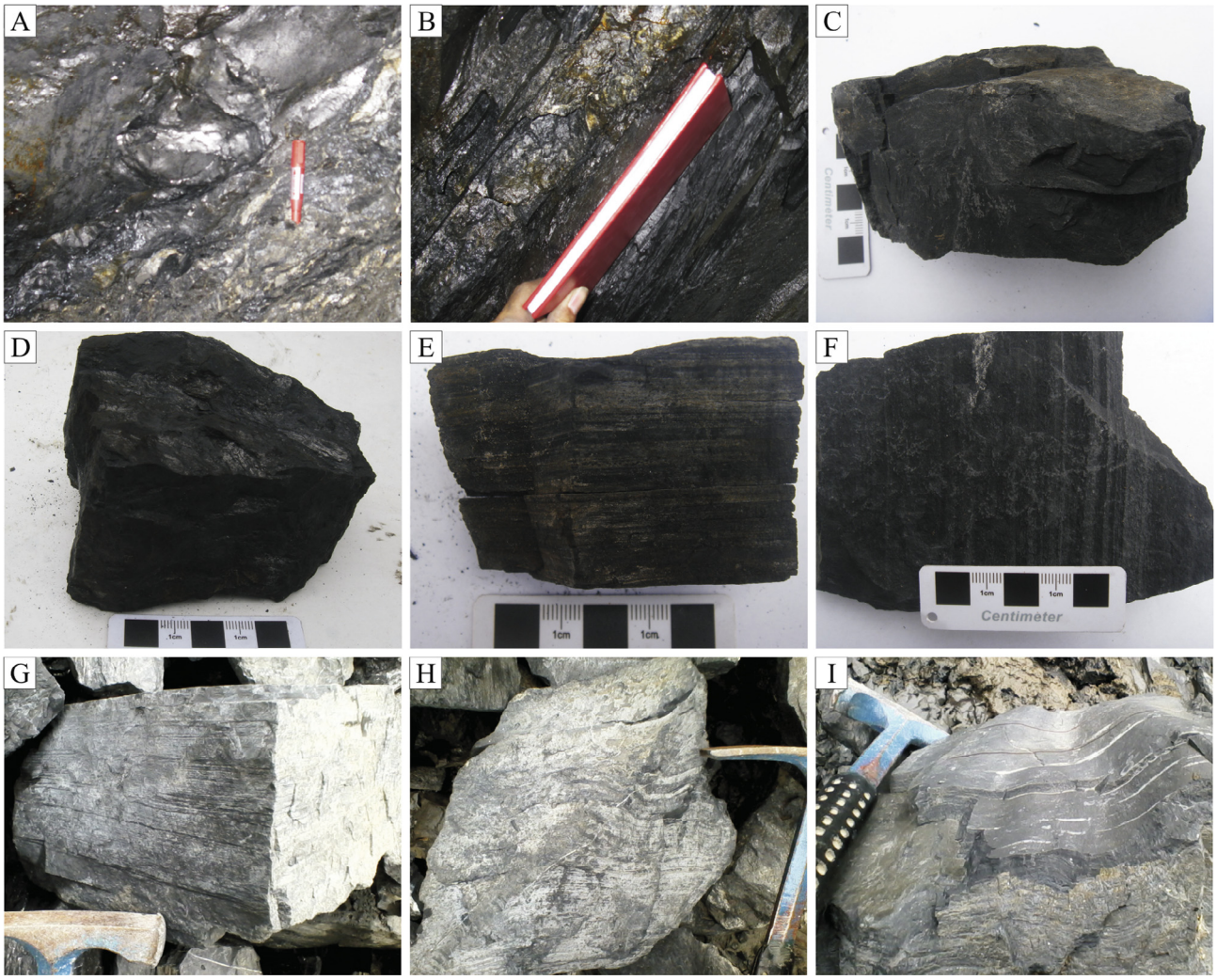

Fig. 3. The morphologies of ore bodies, typical ores and sedimentary structures on Datangpo-type manganese ores in northeastern Guizhou and It's adjacent areas. A: Lenticular body; B: Stratiform-like body; C, D: Massive ore (structure); E, F: Banded ore (structure); F: Horizontal bedding; H: Wavy bedding; I: Wavemark.

bedding (Fig. 3G) consisting of interphase light and dark lamina. Additionally, wavy bedding (Fig. 3H) and wavemark (Fig. 3I) have also developed.

3. Materials and analytical methods

The Datangpo-type manganese ore samples were collected from a series of different deposits, including the Yanglizhang deposit (28°4′14.36″N, 108°46′3.66″E, five samples), Songtao County, Guizhou province, the Minle deposit (28°22′30.5″N, 109°20′10.5″ E, four samples), Huayuan County, Hunan province, and the Rongxi deposit (28°32′35.5″N, 108°48′58″E, five samples), Xiushan County, Chongqing City. A few wall rocks (black shale) were collected to compare to manganese ores. All of the samples were fresh (i.e., did not contain secondary veins) and were crushed to a size of 200 mesh for analyses of major and rare earth elements.

Major components, including SiO_2, Al_2O_3, TiO_2, TFe, MnO, CaO, MgO, K_2O, and P_2O_5, were analyzed through X-ray fluorescence analysis by ALS Minerals (Guangzhou) Co., Ltd.

Rare earth elements (REE, including lanthanide elements and yttrium) were analyzed by ICP-MS using a PerkinElmer ELAN DRC-e quadrupole inductively coupled plasma mass spectrometer (Q-ICP-MS) with a relative standard deviation of generally better than 5% at the State Key Laboratory of Ore Deposit Geochemistry of the Institute of Geochemistry, Chinese Academy of Science. The Ce, Eu and Y anomalies were calculated using the following formulas: $Ce_{anom.} = (Ce/Ce^*)_{SN} = 2Ce_{SN}/(La_{SN} + Pr_{SN})$, $Eu_{anom.} = (Eu/Eu^*)_{SN} = 2Eu_{SN}/(Sm_{SN} + Gd_{SN})$, and $Y_{anom.} = (Y/Y^*)_{SN} = 2Y_{SN}/(Dy_{SN} + Ho_{SN})$, where $_{SN}$ represents the normalization of concentrations against those of the PAAS shale standard (Post-Archean Australian Shale, Taylor and McLennan, 1985).

To make the results more representative, geochemical data of major elements and REE of other Datangpo-type Mn deposits, such as Daotuo (An et al., 2014; nine samples) and Xixibao (He et al., 2013; Zhang, 2014; eleven samples), were also referenced. These data were published after 2010; the analytical results of the manganese ore samples collected from different deposits served as basic information for this analysis.

In addition, before conducting geochemical analyses, polished thin sections of samples were analyzed to identify the mineral components and microscopic structures of manganese ores and black shale using a JEOL JSM-6460lv scanning electron microscope at the State Key Laboratory of Environmental Geochemistry at the Institute of Geochemistry, Chinese Academy of Science. This allowed us to obtain back-scattered electron (BSE) images and energy dispersive spectrometry (EDS) qualitative analyses of Mn carbonate and detrital minerals.

4. Mineralogical components

The SEM photographs of the polished thin sections show that manganese ores consist chiefly of terrigenous minerals, manganese-bearing carbonates and some authigenic minerals (Fig. 4A). Most of the terrigenous minerals are quartz minerals, with small quantities of feldspar, mica and clay minerals (Fig. 4B). Manganese-bearing manganese carbonate minerals mainly include rhodochrosite and calico-rhodochrosite grains. Single manganese carbonate grains have a globular shape, a uniform size of approximately 5 μm, a pure inner structure and a rare girdle structure (Fig. 4C, D). The energy dispersive spectrometry (EDS) qualitative analyses show that Mn, Ca, and Mg are the main cations present, and that the sum of these cations is stable and constant, implying that they are isomorphic replacements of one another. Terrigenous minerals form darker assemblages whereas manganese carbonate mineral grains form bright assemblages. In addition, the boundary between the different assemblages is pronounced. Pyrite, which is the main authigenic mineral, is primarily globular and framboidal (Fig. 4B, E) and is abundant in assemblages of terrigenous minerals but rare in assemblages of manganese-bearing manganese carbonate minerals, thus showing close associations with terrigenous minerals (Fig. 4A, E).

Based on the relative proportions of terrigenous minerals and manganese-bearing carbonate minerals, the manganese ores can be subdivided into two types: (1) massive manganese ores that

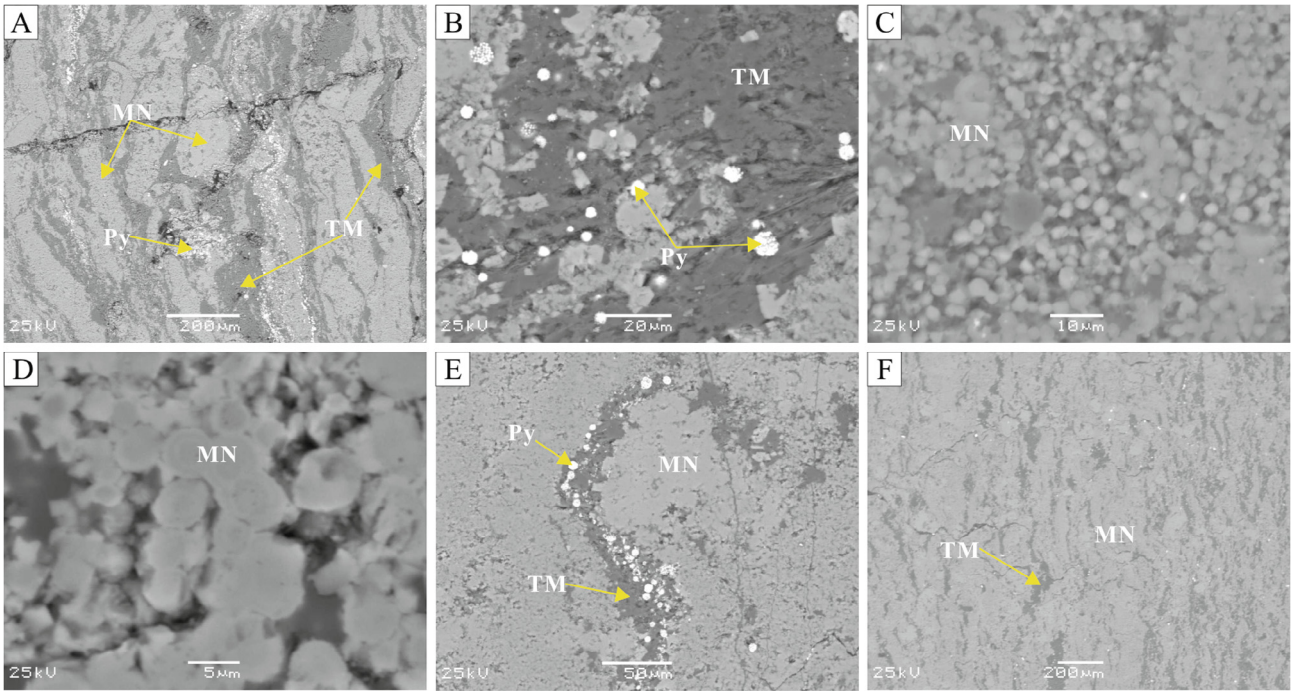

Fig. 4. SEM-BSE images of thin sections of manganese ores. In all images, relatively light gray minerals are manganese-bearing carbonates (MN), relatively dark gray minerals are terrigenous minerals (TM), and bright minerals are pyrite (Py). A: Ribbon-shaped manganese ore with a light gray layer (manganese-rich carbonate) and dark gray layer (composed of terrigenous minerals); pyrite was mainly found in the terrigenous mineral layer. B: Dark assemblage of terrigenous minerals with globular and framboidal pyrites. C: Manganese-bearing carbonate grains of uniform size. D: The inner girdle structure of a single manganese carbonate grain. E: Globular and framboidal pyrites found in assemblages of terrigenous minerals. F: Massive manganese ores chiefly composed of manganese carbonate grains with rare terrigenous minerals and pyrite.

Table 2
Major element content (wt%) of Datangpo-type manganese ores and black shales.

Deposit	Sample NO.	Lithology	SiO_2	TiO_2	Al_2O_3	TFe	MnO	CaO	MgO	Na_2O	K_2O	P_2O_5	Mn/Fe*
Yanglizhang	YLZ-1	Mn ore	5.76	0.12	1.97	3.19	39.81	6.26	4.40	0.20	0.55	0.93	13.82
	YLZ-2	Mn ore	26.73	0.35	7.22	3.61	22.46	8.46	2.00	0.96	1.83	0.75	6.89
	YLZ-3	Mn ore	18.11	0.13	4.59	3.01	30.45	7.32	3.41	0.41	1.23	0.34	11.20
	YLZ-4	Mn ore	17.39	0.30	5.51	4.70	27.45	8.76	2.61	0.64	1.45	1.75	6.47
	YLZ-5	Mn ore	18.69	0.23	4.95	3.31	27.64	9.09	2.95	0.52	1.32	0.60	9.25
	YLZ-6	Black shale	60.99	0.44	12.34	2.76	5.88	1.77	1.20	1.58	3.11	0.16	2.13
Minle	ML-1	Black shale	76.00	0.42	11.50	2.61	0.11	0.64	0.52	2.17	2.48	0.24	0.04
	ML-2	Mn ore	12.31	0.18	2.50	2.57	31.82	10.78	3.77	0.36	0.65	0.31	13.71
	ML-3	Mn ore	14.46	0.15	2.06	2.32	32.84	7.91	4.18	0.43	0.50	0.27	15.67
	ML-4	Mn ore	12.20	0.15	2.21	2.27	32.07	10.55	3.66	0.32	0.58	0.31	15.64
	ML-5	Mn ore	13.38	0.16	2.95	3.15	34.49	5.84	3.79	0.30	0.81	0.29	12.12
	ML-6	Black shale	68.71	0.40	10.74	6.12	1.00	1.65	0.83	2.04	2.32	0.21	0.13
Rongxi	RX-1	Mn ore	24.49	0.31	5.83	3.31	27.52	5.86	2.67	0.77	1.26	0.60	9.21
	RX-2	Black shale	60.54	0.62	15.84	5.40	0.23	0.61	0.88	1.64	3.92	0.26	0.04
	RX-3	Mn ore	25.23	0.38	6.37	3.73	23.20	8.16	2.15	0.70	1.55	0.55	6.89
	RX-4	Mn ore	11.28	0.15	2.34	2.72	30.32	12.74	2.75	0.28	0.57	0.45	12.34
	RX-5	Mn ore	22.06	0.31	5.53	3.86	24.63	9.44	2.26	0.63	1.28	0.50	7.07
	RX-6	Mn ore	19.45	0.24	4.27	3.76	26.76	9.98	2.68	0.51	1.04	0.34	7.88

*Mn/Fe stands for the radio of MnO to TFe.

are chiefly composed of manganese carbonate grains, rare terrigenous minerals and pyrite (Fig. 4F); and (2) ribbon manganese ores with a light gray manganese carbonate mineral layer and a dark gray terrigenous mineral layer, containing abundant pyrite that mainly occurs in the terrigenous mineral layer (Fig. 4A).

5. Geochemical rock compositions

5.1. Major element geochemistry

The main elemental compositions of the Datangpo-type manganese ore and black shale samples are listed in Table 2. MnO and SiO_2 are the main elements found in these Mn ores, with average values of 29.39% and 17.25%, respectively. The average values of the other main elements (Al_2O_3, TiO_2, Na_2O and K_2O) are 4.16%, 0.23%, 0.50% and 1.04%, respectively. The average values of Cao, MgO and P_2O_5 are 8.65%, 3.09% and 0.57%, respectively. However, SiO_2 and Al_2O_3 are the main components of the black shales, with average values of 66.56% and 12.61, respectively. The other elements (TiO_2, Na_2O and K_2O) have average values of 0.47%, 1.86% and 2.96%, and MnO, CaO, MgO and P_2O_5 have average values of 1.81%, 1.17%, 1.86%, 0.22%, respectively. TFe accounts for 3.35% and 4.22% of the Mn ores and black shales, respectively.

Consequently, Mn ores are relatively more abundant in MnO, CaO, MgO and P_2O_5 and less abundant in Al_2O_3, SiO_2, TiO_2, TFe, Na_2O and K_2O than the black shales. The Mn ores also have a high Mn/Fe ratio, with an average value of 9.56, thus recording higher levels of fractionation between Mn and Fe.

5.2. REY (REE + Y) geochemistry

The contents of rare earth elements and some parameters of the Datangpo-type manganese ore and black shale samples are shown in Table 3. The total REY content (∑REY) records a relatively large and variable range of 170.27 to 515.68 ppm, with an average value of 255.24 ppm, which is higher than that of the Post-Archean Australian Shale (210.00 ppm). The value of $(Ce/Ce^*)_{SN}$ varies from 1.160 to 1.368, with an average value of 1.253, and the value of $(Ce/Pr)_{SN}$ varies from 1.080 to 1.369, with an average value of 1.207, thus recording prominent positive Ce anomalies. The value of $(Eu/Eu^*)_{SN}$ varies from 0.92 to 1.493, with an average value of 1.152, thus representing weak to strong positive Eu anomalies. In addition, $(Y/Y^*)_{SN}$ varies from 0.83 to 0.996, with an average value of 0.893. However, measured $(Y/Ho)_{SN}$ ratios vary from 0.89 to 1.066, with an average value of 0.965. As this value is close to 1, Y anomalies are negligible and may result from positive Dy anomalies.

Moreover, the PAAS-normalized distribution patterns of the rare earth elements (REY_{SN}) of manganese ores are characterized by the pronounced enrichment of middle rare earth elements (MREEs) compared to those of both LREE and HREE, producing a "hat-shaped" REY plot (Fig. 5). Consequently, Datangpo-type manganese ores are characterized by relative MREE enrichment, prominent positive Ce anomalies, weak to strong positive Eu anomalies, and negligible negative Y anomalies (Fig. 5), thus complementing the results of previous studies (e.g., An et al., 2014; Zhu et al., 2013). In addition, the REY characteristics of Mn ores are similar to those of other Datangpo-type Mn ores, such as the Daotuo and Xixibao manganese deposits (Fig. 6), indicating that they may have undergone similar ore-forming processes.

The ∑REY of country rocks range from 107.41 to 196.7 ppm, with an average value of 148.34 ppm, which is less than the average of Mn ores (255 ppm) and the average of PAAS (210 ppm). The PAAS-normalized distribution patterns of the rare earth elements (REY_{SN}) of the country rocks are characterized by the slight enrich-

Table 3
REY content (ppm) and some parameters of Datangpo-type manganese ores and black shales.

Deposit	Sample NO.	La	Ce	Pr	Nd	Sm	Eu	Gd	Tb	Dy	Y	Ho	Er	Tm	Yb	Lu	∑REY	$(Ce/Ce^*)_{SN}$	$(Eu/Eu^*)_{SN}$	$(La/Pr^*)_{SN}$	$(Y/Ho^*)_{SN}$	$(Y/Y^*)_{SN}$
Yanglizhang	YLZ-1	23.30	72.10	7.34	34.80	8.15	1.56	7.31	1.23	6.63	33.30	1.29	3.09	0.41	2.27	0.29	203.07	1.254	0.941	0.743	0.956	0.882
	YLZ-2	39.60	96.40	8.91	35.00	6.41	1.15	4.93	1.01	5.79	31.10	1.15	3.57	0.55	3.11	0.40	239.08	1.180	0.952	1.041	1.002	0.934
	YLZ-3	82.00	212.0	19.9	76.60	14.80	2.75	13.09	2.38	12.80	63.20	2.34	6.99	0.92	5.21	0.69	515.68	1.206	0.922	0.965	1.000	0.892
	YLZ-4	52.90	135.0	13.5	56.30	11.30	2.19	9.53	1.66	9.44	54.10	1.88	5.65	0.83	4.55	0.61	359.44	1.160	0.985	0.918	1.066	0.996
	YLZ-5	45.4	116	11.7	51.7	11.6	1.80	10.0	1.88	10.4	59.0	2.19	6.22	0.98	5.62	0.75	335.26	1.156	0.780	0.909	0.998	0.960
	YLZ-6	14.8	36.3	3.42	14.3	3.13	0.34	2.84	0.56	3.8	19.8	0.83	2.95	0.45	3.38	0.51	107.41	1.177	0.531	1.000	0.871	0.887
Minle	ML-1	25.6	51.8	5.6	22	4.37	0.72	3.12	0.64	3.59	19.3	0.81	2.49	0.35	2.58	0.43	143.40	0.998	0.918	1.057	0.878	0.904
	ML-2	29.00	81.50	6.71	27.30	5.69	1.56	4.84	0.83	5.08	26.80	1.11	3.28	0.44	2.52	0.37	197.02	1.343	1.388	1.012	0.894	0.877
	ML-3	23.50	69.20	5.75	23.50	4.71	1.45	4.33	0.81	4.90	25.50	1.00	2.87	0.41	2.07	0.28	170.27	1.368	1.493	0.957	0.944	0.894
	ML-4	25.30	70.50	5.73	24.30	5.04	1.24	4.52	0.81	4.43	25.00	0.90	2.58	0.36	2.14	0.29	173.13	1.346	1.208	1.034	1.031	0.972
	ML-5	31.20	90.30	7.71	33.40	7.75	1.61	6.68	1.19	6.46	30.80	1.26	3.54	0.49	2.85	0.38	225.62	1.338	1.045	0.948	0.905	0.836
	ML-6	32.5	76.5	8.71	35.5	6.24	1.08	4.40	0.77	3.83	20.7	0.82	2.24	0.43	2.59	0.40	196.70	1.046	0.970	0.863	0.925	0.931
Rongxi	RX-1	26.60	72.90	6.89	30.80	6.57	1.49	6.03	1.08	6.02	30.20	1.18	3.51	0.51	3.03	0.42	197.23	1.236	1.101	0.904	0.948	0.878
	RX-2	26.9	51.6	5.16	20.1	3.89	0.69	3.80	0.61	3.76	21.3	0.87	2.76	0.46	3.43	0.54	145.85	1.006	0.842	1.205	0.904	0.941
	RX-3	34.70	93.10	9.06	40.50	8.49	2.20	8.31	1.47	8.38	40.60	1.63	4.56	0.62	3.49	0.52	257.63	1.205	1.218	0.897	0.923	0.851
	RX-4	33.60	89.20	9.20	39.90	9.44	2.64	9.01	1.55	8.98	47.20	1.71	4.69	0.67	3.69	0.51	261.99	1.163	1.335	0.855	1.022	0.932
	RX-5	27.40	78.70	7.64	35.00	8.46	2.10	7.89	1.39	7.96	38.20	1.56	4.20	0.53	3.43	0.52	224.98	1.246	1.198	0.840	0.907	0.840
	RX-6	44.40	123.0	11.50	47.50	9.18	2.17	7.91	1.22	6.87	31.00	1.21	3.49	0.44	2.74	0.38	293.00	1.250	1.185	0.904	0.949	0.829

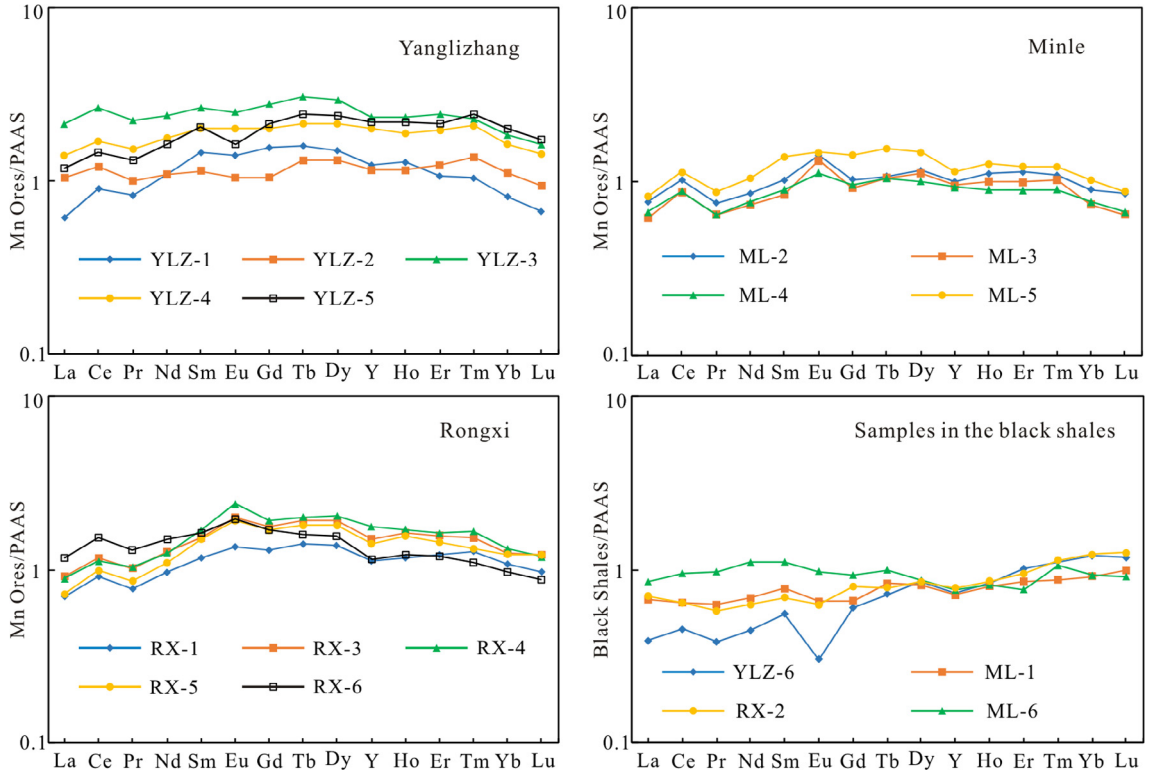

Fig. 5. Post-Archean Australian Shale-normalized REY patterns of Mn ores and black shales in Yanglizhang, Minle and Rongxi manganese deposits.

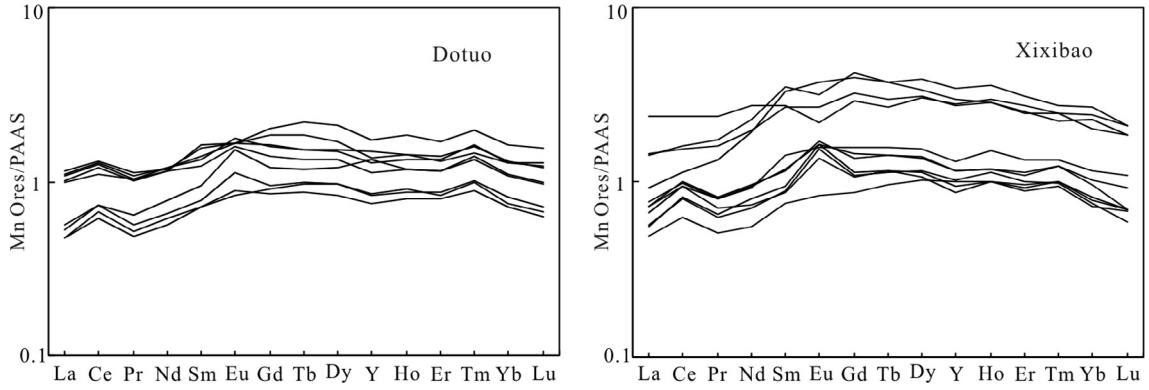

Fig. 6. Post-Archean Australian Shale-normalized REY patterns of Mn ores in the Daotuo and Xixibao manganese deposits.

ment of HREE, producing a "flat-shaped" REY plot, showing no Ce anomalies (with an average value of 1.06), weakly negative Eu anomalies (with an average value of 0.82), weakly negative Y anomalies (with an average value of 0.92), variable $(Pr/Yb)_{SN}$ values (ranging from 0.32 to 1.07, with an average value of 0.64), and HREE enrichment relative to LREE.

6. Analysis of the formation processes of manganese ore

6.1. Ce anomalies

Rare earth elements constitute a group of elements that exhibit generally similar geochemical behaviors and trivalent ions, but vary in terms of their Ce^{4+} and Eu^{2+} stability within oxidizing and reducing environments, respectively (Holser, 1997). Hence, Ce and Eu are the only redox-sensitive rare earth elements. In oxic marine environments, soluble Ce^{3+} is oxidized into insoluble Ce^{4+} as CeO_2 and tends to be rapidly removed from seawater via scavenging by Fe and Mn oxyhydroxides or by organic matter in suspension, thus producing a strong negative Ce anomaly in the modern surface oxidizing water column (Holser, 1997; Pourret et al., 2008; Xiong et al., 2012). In suboxic/anoxic marine environments, insoluble CeO_2 is reduced and remobilized to soluble Ce^{3+}, which behaves similarly to other trivalent REEs, producing a weak or negligible negative Ce anomaly or even slightly positive Ce anomalies in REE distributions (Bau et al., 1997; Holser, 1997; Wilde et al., 1996). However, studies have shown that the kinetics of Ce^{3+} oxidation reactions are slow and can usually be overcome via microbial mediation or through surface-catalysis on Mn oxides and hydrous Fe oxides (Bau and Koschinsky, 2009; Moffett, 1990, 1994; Pourret et al., 2008, and references therein). Based on the sequential leaching procedures of some ferromanganese crusts, Bau and Koschinsky (2009) suggested that the preferential removal of Ce from seawater does not result from the oxidation of dissolved Ce^{3+} within the marine water column, but rather that Ce^{3+} is

oxidized after its sorption at the metal oxyhydroxide surface. In any case, the development of a Ce anomaly is most closely associated with preferential scavenging by Fe and/or Mn oxides and organic matter (e.g., Alibo and Nozaki, 1999; Bau and Koschinsky, 2009; De Carlo et al., 1997; Ohta and Kawabe, 2001; Pourret et al., 2008). Consequently, manganese-bearing sediments forming in oxic marine environments, and hydrogenetic Fe-Mn nodules and crusts in particular, are characterized by prominent positive Ce anomalies (e.g., Bau et al., 1996, 2014; Cui et al., 2009; Kunzendorf et al., 1993; Pattan et al., 2005; Surya Prakash et al., 2012).

However, it is possible that Ce anomalies can result from La anomalies, due to the fact that Ce anomalies are calculated from the following equation: $Ce_{anom.} = (Ce/Ce^*)_{SN} = 2Ce_{SN}/(La_{SN} + Pr_{SN})$. To avoid this, Bau and Dulski (1996) introduced the $(Ce/Ce^*)_{SN}$ *vs.* $(Pr/Pr^*)_{SN}$ diagram to judge whether Ce anomalies are exaggerated by the La effect, noting that the $(Pr/Pr^*)_{SN}$ is calculated from the following equation: $(Pr/Pr^*)_{SN} = 2Pr_{SN}/(Ce_{SN} + Nd_{SN})$. As there is no chemical premise for the creation of Nd or Pr anomalies, the existence of a true Ce anomaly should yield values of $(Pr/Pr^*)_{SN} > 1$ or $(Pr/Pr^*)_{SN} < 1$. If, however, samples record values of $(Pr/Pr^*)_{SN} \approx 1$, this implies that the anomalous enrichment or depletion of La must be the sole cause of Ce anomalies. Fig. 7 shows that the Ce anomalies of manganese ores are real and do not record the effects of La (Bau and Dulski, 1996; Shields and Stille, 2001). Sample $(La/Pr)_{SN}$ values range from 0.74 to 1.041 with an average value of 0.925. With the exception of the YLZ-1 samples ($(La/Pr)_{SN} = 0.74$), the $(La/Pr)_{SN}$ values of the other samples are close to 1, denoting that La anomalies are nonexistent and that the observed positive Ce anomalies are genuine.

Furthermore, these positive Ce anomalies show a strong positive correlation with MnO concentrations within Datangpo-type manganese ores (Fig. 8a); therefore, we suggest that the enrichment of Ce is controlled by MnO content. Manganese is oxidized into insoluble Mn (III) and Mn (IV) oxides (Calvert and Pedersen, 1993, 1996), which are then precipitated into the oxic marine water column through the adsorption of relatively high contents of Ce during deposition, based on the close relationship between positive Ce anomalies and the oxidative scavenging of cerium by Mn oxides (e.g., Bau and Koschinsky, 2009; De Carlo et al., 1997; Ohta and Kawabe, 2001). Here, the Mn (III) and Mn (IV) solid phases, which are referred to as Mn-oxyhydroxides, are mainly MnOOH and MnO_2 (Tribovillard et al., 2006).

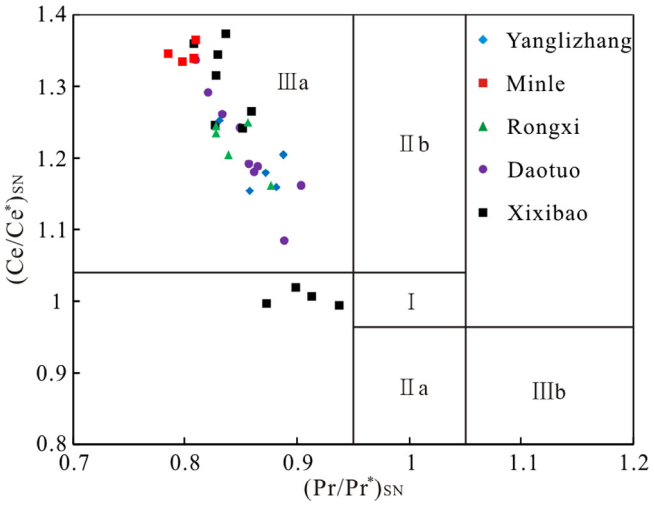

Fig. 7. $(Ce/Ce^*)_{SN}$ vs. $(Pr/Pr^*)_{SN}$ diagram of Datangpo-type manganese ores (Bau and Dulski, 1996). Field I: neither Ce nor La anomaly, field IIa: positive La anomaly, no Ce anomaly, field IIb: negative La anomaly, no Ce anomaly, field IIIa: real positive Ce anomaly, field IIIb: real negative Ce anomaly.

6.2. Eu anomalies

Theoretically speaking, Eu exhibits similar geochemical behavior as other REEs, although it is oxidized to Eu^{3+} in oxic environments and converted to Eu^{2+} in reducing environments (Holser, 1997). The low-temperature aqueous geochemistry of europium is dominated by Eu^{3+} and its related complexes in seawater, oxygenated meteoric water, rivers and rain (Sverjensky, 1984). However, Eu is not as significantly fractionated as cerium during precipitation-dissolution processes (Shields and Stille, 2001). Based on thermochemical analyses, Sverjensky (1984) suggested that the relative stabilities of aqueous Eu^{2+} and Eu^{3+} are closely associated with a wide range of temperatures, pressures and Eh-pH conditions, and reactions that involve transferring Eu^{3+} to Eu^{2+} include the following characteristics. (1) Under high temperatures (greater than 250 °C) and high pressures, divalent europium predominates, and hydrothermal fluids and sediments of hydrothermal origin are usually characterized by their obvious positive Eu anomalies (Bau and Dulski, 1995; Douville et al., 1999; Olivarez and Owen, 1991). (2) Under low temperatures (approximately 25 °C), close to that of the Earth's surface, europium is dominated by a divalent state in most reducing alkaline pore waters of anoxic marine sediments. Positive Eu anomalies resulting from the participation of Eu^{2+} in the crystal lattices of sulfates or carbonate minerals are closely related to sulfate reduction and the degradation of organic matter during early diagenetic processes. In turn, a few cases of positive Eu anomalies have been reported in low-temperature environments, which are mostly associated with organic-rich, sulfate-reducing sediments or sedimentary rocks (Kidder et al., 2003; Maceae et al., 1992; Martinez-Ruiz et al., 1999; Xiong et al., 2012).

Weak to strong positive Eu anomalies appearing in manganese ores may result from the reducing alkaline environments in anoxic pore waters found during post-depositional diagenetic processes, since analysis of the SiO_2-Al_2O_3 concentration diagram, in which most data plot within a normal sedimentary range, excludes the possibility that positive Eu anomalies can result from hydrothermal activity (Fig. 8b). This is consistent with the relatively high levels of organic carbon content found in the first member of Datangpo Formation. Positive Eu anomalies show relatively strong positive correlations with MnO, CaO, and MgO contents (Fig. 8c), indicating that Eu^{2+} is formed by the reduction of Eu^{3+} in reducing alkaline pore waters, which then participates in the crystal lattices of carbonate minerals by substituting for Mn, Ca and Mg cations, thus further enriching their Eu concentrations and positive Eu anomalies.

Moreover, according to the $\sum$REY-Al_2O_3 concentration diagram (Fig. 8d), the total REY and Al_2O_3 contents show a clear positive correlation, in which the slope of the regression line is greater than that of the ligature line between the PAAS point and the coordinate origin, and the intercept of the regression line is greater than zero. These features indicate that the REY record origins other than that of terrigenous detrital input, and they also imply that REY redistribution can occur during early diagenetic processes.

6.3. Y anomalies

The development of a Y anomaly in natural waters is often related to the lower particle-reactivity of Y compared to those of the other REE (especially its REE neighbors) (Bau and Koschinsky, 2009; Bau et al., 1996, 1997). When high-temperature hydrothermal fluids are mixed with entrained seawater, REE is partly scavenged by Fe oxyhydroxides, whereas Y is not affected,

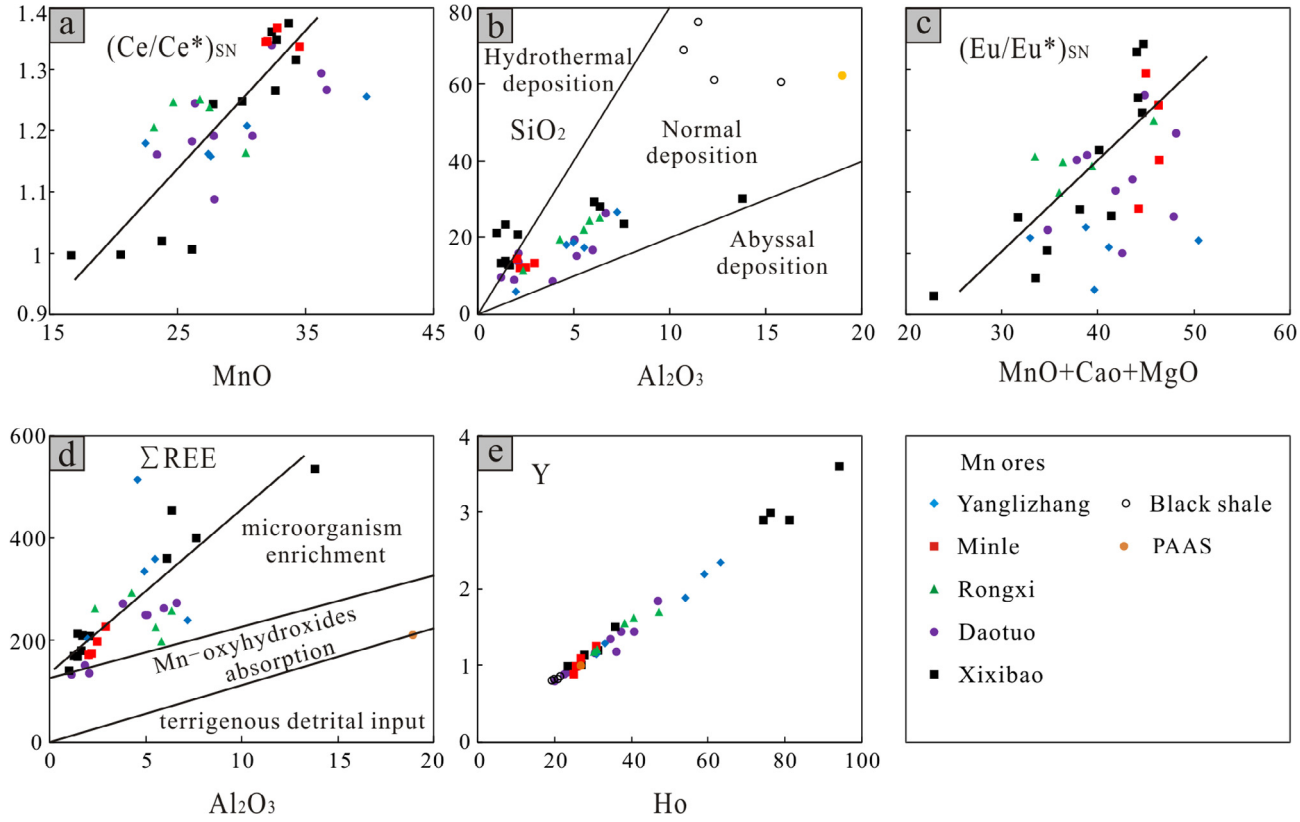

Fig. 8. Binary plots between major elements: (a) $(Ce/Ce^*)_{SN}$ *vs.* MnO, (b) SiO_2 *vs.* Al_2O_3, (c) $(Eu/Eu^*)_{SN}$ *vs.* (MnO + CaO + MgO), and (d) ∑REE *vs.* Al_2O_3 and (e) Y *vs.* Ho to illustrate differences in the geochemistry of the Mn ores relative to different manganese deposits.

in marked contrast to REE behavior (Bau and Dulski, 1999; Douville et al., 1999). However, under normal depositional conditions, pronounced Y-Ho fractionation often results from the preferential sorption of Ho with respect to Y by Fe- and Mn-oxyhydroxide particles, due to the lower stability of surface complexes of Y relative to those of Ho during the redox-cycling of Mn and Fe (Bau et al., 1996, 1997). Therefore, seawater usually records prominent positive Y anomalies and higher Y/Ho ratios, whereas negative Y anomalies and lower Y/Ho ratios are common among manganese-bearing sediments (Bau et al., 1996, 1997, 2014; Surya Prakash et al., 2012).

However, the Y anomalies of manganese ores are very weak (likely negligible) and presumably result from positive Dy anomalies. In addition, the Y/Ho ratios of manganese ores are very close to those of PAAS (Fig. 8e); values of $(Y/Ho)_{SN}$ range from 0.89 to 1.066, with an average value of 0.965, thus illustrating the fractionation of Y-Ho resulting from the preferential sorption of Ho compared to that observed when the sorption of Y by Fe- and/or Mn-oxyhydroxide particles is not considered (Fig. 8e). This may be attributable to the shallower basin water columns and/or faster sedimentary rates found in epicontinental semi-limited shallow basins, which limit the residence time needed for Mn-oxyhydroxides in water columns to produce obvious Y-Ho fractionation in the absence of hydrothermal activity.

6.4. REY origins

The absorption of REY from ambient seawater by Mn-oxyhydroxides occurs during deposition, when manganese is precipitated as Mn-oxyhydroxide in the oxygenated water column (Koeppenkastrop and De Carlo, 1992, 1993; Koschinsky and Hein, 2003; Pourret and Davranche, 2013, and references therein). This can be demonstrated by the intercept (greater than zero) of the regression line in a ∑REY-Al_2O_3 concentration diagram (Fig. 8D), which denotes the lowest content of REY derived from absorption by Mn-oxyhydroxides. There are relatively high levels of P_2O_5 in manganese ores, and partial REY content initially derived from organic matter should be taken into consideration, as microorganism activity can lead to the enrichment of REY from ambient seawater (Pi et al., 2013). Hence, REY in manganese ores is mainly derived from three origins: terrigenous detrital input, absorption by Mn-oxyhydroxides and microorganism enrichment (Fig. 8d).

In addition, the redistribution of REY during the post-depositional diagenetic stage is confirmed by the positive correlation between total REY and Al_2O_3 contents in the ∑REY-Al_2O_3 diagram (Fig. 8d), which suggests that the REY derived from absorption by Mn-oxyhydroxides and the enrichment of microorganisms should be released into interstitial water along with the degradation of organic matter and the reductive dissolution of Mn-oxyhydroxides. Under reducing alkaline conditions, Ce^{2+} is derived from the reductive dissolution of CeO_2, and Eu^{2+} is transferred from the reduction of Eu^{3+} and is substituted for Mn, Ca and Mg during the formation of rhodochrosite. All of the rare earth elements participate in the formation of authigenic clay minerals as trivalent cations, thus creating a close correlation between the total REY and Al_2O_3 contents in manganese ores.

6.5. Genetic processes of Mn ores

Based on the above analyses, we suggest that manganese was oxidized into Mn-oxyhydroxide particles in oxic water, likely at a faster sedimentary rate, during the mineralization stage. In an early diagenetic stage, pore water gradually became anoxic due to the degradation of organic matter. An oxidizing agent, such as

nitrate, Fe-Mn-oxyhydroxides, or phosphate (listed in order of oxidizing capacity), participated in the degradation of organic matter by substituting O_2 when soluble oxygen ran out (Tribovillard et al., 2006). Therefore, Mn-oxyhydroxides were reduced to soluble Mn^{2+} along with the degradation of organic matter and preserved in closed pore water after Mn was oxidized to form insoluble Mn-oxyhydroxides, which were buried with algae microorganisms under oxic conditions. Soluble CO_2 in pore water was characterized by enriched light isotopes formed by the mixture of CO_2 from the degradation of organic matter and the soluble CO_2 of sea water. The partial dissolution of CO_2 formed HCO_3^- in pore water under higher pressure, and manganese carbonate-rhodochrosite formed due to the combination of Mn^{2+} and HCO_3^- along with the gradual increase of the ionic concentration of pore water (Calvert and Pedersen, 1993, 1996; Tribovillard et al., 2006).

In addition, REY absorbed by Mn-oxyhydroxides during sedimentation and enriched in microbial organisms were released into pore water, where Ce^{4+} was reduced to Ce^{2+} and Eu^{3+} was reduced to Eu^{2+}. Ce^{2+} and Eu^{2+} entered the lattices of carbonate minerals while other REE entered those of authigenic clay minerals, such as montmorillonite or illite lattices, as trivalent REEs (REE^{3+}).

7. Genetic types and REY geochemistry of marine Fe-Mn oxyhydroxides

Studies show that genetic Cenozoic marine Fe-Mn oxyhydroxide precipitates are commonly subdivided into three discrete types: hydrothermal, hydrogenetic, and diagenetic (Takematsu et al., 1989; Usui and Terashima, 1997). These Fe-Mn oxyhydroxide precipitates include hydrothermal deposits (crusts), hydrogenetic crusts, hydrogenetic nodules, diagenetic nodules and phosphatized crusts (e.g., Bau et al., 1996, 2014; Halbach et al., 1981; Jeong et al., 2000; Koschinsky et al., 1997). Due to their different formation environments and growth processes, these Fe-Mn oxyhydroxide precipitates have different mineralogical components and geochemical compositions (e.g., manganese-bearing mineral types; Mn/Fe ratios; contents of transition metals such as Cu, Co, Ni, Zn, Ba, Gd, Zn; and contents and distribution patterns of REY) (Bau et al., 1996; Cui et al., 2009; De Carlo et al., 1987; Moorby et al., 1984; Surya Prakash et al., 2012; Takematsu et al., 1989; Usui and Terashima, 1997, and references therein). Geochemical features, particularly the contents and distribution patterns of REY, are the main indicators used to identify different genetic types of marine Fe-Mn oxyhydroxide precipitates (Fig. 9). The formation environments, growth processes, mineralogical components and geochemical compositions (particularly REY) of different genetic types of marine Fe-Mn oxyhydroxide precipitates are described as follows.

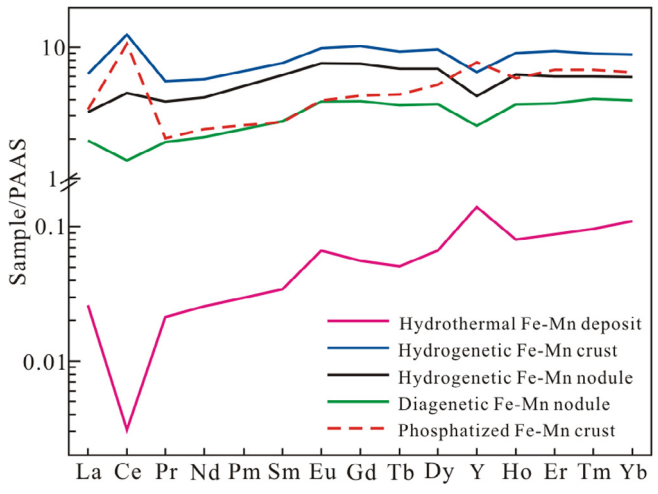

Fig. 9. Post-Archean Australian Shale-normalized REY (REE + Y) patterns of different genetic forms of modern marine ferromanganese oxyhydroxide precipitates (Bau et al., 2014).

7.1. Hydrogenetic Fe-Mn crusts and nodules

Hydrogenetic Fe-Mn crusts and nodules are composed of Fe-Mn oxyhydroxides or colloidal particles, which precipitate through normal seawater sedimentation (Bau et al., 2014; Roy, 1992). Crusts and nodules differ in their formation positions. Fe-Mn crusts grow along the surfaces of solid substrates and form in topographically high positions where bottom currents are strong enough to remain free of sediments for millions of years (e.g., seamount basalts, inactive seamounts, plateaus, ridges, and hills in ocean basins) (Canet et al., 2008; Takematsu et al., 1989; Usui and Terashima, 1997). In contrast, Fe-Mn nodules grow via accretion around a nucleus of soft sediment and are exposed to pelagic clay (Takematsu et al., 1989; Wegorzewski and Kuhn, 2014). They are characterized by very slow growth rates of less than ten millimeters per million years (Bau et al., 2014; Usui and Terashima, 1997) and by smaller Mn/Fe ratios (ranging from 0.5 to 2), typically due to the relatively stable chemical compositions of modern seawater (Bau and Koschinsky, 2009; Canet et al., 2008; Cui et al., 2009). Mineralogically, hydrogenetic nodules and crusts are dominated by an amorphous FeOOH phase that is closely intergrown with poorly crystalline Fe-bearing vernadite (δ-MnO_2) (Bau et al., 1996; Kuhn et al., 1998; Surya Prakash et al., 2012; Takematsu et al., 1989; Usui and Terashima, 1997). Fe-Mn oxyhydroxides are found in seawater as initial colloidal particles with a surface charge, such as slightly positively surface-charged Fe oxides and negatively surface-charged Mn oxides (Bau and Koschinsky, 2009; Surya Prakash et al., 2012, and references therein).

According to the "simplified electrostatic" model (also referred to as the SES model), positively charged dissolved species are preferentially combined with Mn oxides that have a negative surface charge in seawater, whereas negatively charged and uncharged dissolved species prefer to be combined with slightly positively surface-charged Fe oxides (Bau and Koschinsky, 2009; Koschinsky and Hein, 2003, and references therein). In addition, dissolved REE in seawater are mostly present as free ions (REE^{3+}) or as mono-carbonate ($REE(CO_3)^+$) or di-carbonate ($REE(CO_3)_2^-$) species (Bau and Koschinsky, 2009; Surya Prakash et al., 2012, and references therein). Hence, surface-charged Fe-Mn oxyhydroxide colloidal particles can scavenge numerous trace elements, especially rare earth elements, from seawater through multiple complex mechanisms (e.g., electrostatic attraction and chemical interaction) (Bau and Koschinsky, 2009; Koeppenkastrop and De Carlo, 1992, 1993; Koschinsky and Hein, 2003, and references therein). Vernadite (δ-MnO_2), which is the main Mn-oxide mineral found in hydrogenetic crusts and nodules, has a layered structure that can accommodate various heavy metal cations (Post, 1999; Surya Prakash et al., 2012, and references therein). Therefore, due to their very slow growth rates, the geochemical compositions of hydrogenetic crusts and nodules are characterized by the enrichment of trace elements and often by the enrichment of transition elements, such as Co, Ni, Cu, Zn, and total REY, at high levels of more than 1000 ppm (Bau and Koschinsky, 2009; Koschinsky and Hein, 2003; Takematsu et al., 1989; Usui and Terashima, 1997, Fig. 9).

However, it should also be noted that the REY absorption capacities of Fe-Mn oxyhydroxide colloidal particles vary. To illustrate the REY fractionation that occurs during the growth processes of the hydrogenetic Fe-Mn crust, apparent bulk coefficients for the partitioning of REY can be calculated as follows:

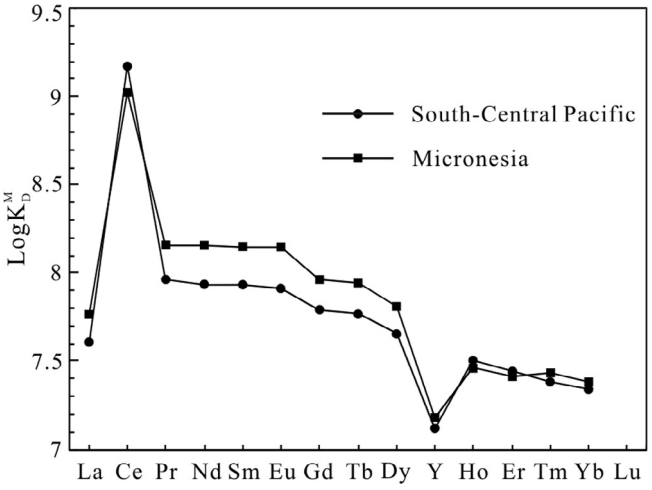

Fig. 10. REY partitioning between hydrogenetic Fe-Mn crusts and seawater (based on Bau et al., 1996, bulk REY partition coefficients are given as log K_D^M and are derived from the mean compositions of South-Central Pacific crusts and crusts from Micronesia).

$$K_D^M = [M]_{FeMnC}/[M] + SW.$$

where K_D^M is the apparent bulk partition coefficient of trace metal M, K_{FeMnC} is the average concentration of M in the hydrogenetic Fe-Mn crust, and $[M]_{SW}$ is the concentration of M in seawater. According to previous studies (Bau and Koschinsky, 2009; Bau et al., 1996; De Carlo and McMurtry, 1992), the apparent bulk partition coefficient of REY features the following characteristics. (1) The partition coefficient of REY tends to decrease from La to Lu. Thus, Fe-Mn oxyhydroxide colloidal particles usually preferentially absorb light rare earth elements. (2) The partition coefficients of Ce are greater than those of other REY, which is likely due to the oxidative scavenging for cerium by Mn and Fe oxides. (3) A distinct decrease in the partition coefficient of Y is related to the lower particle reactivity of Y compared to those of the other REE (Fig. 10).

Consequently, the hydrogenetic Fe-Mn crusts and nodules record prominent positive Ce anomalies and negative Y anomalies (Fig. 9). Some sequential leaching procedures for the hydrogenetic Fe-Mn crusts were also carried out to further examine the REY absorption occurring during different geochemical phases; we thus obtained the REY distributions for four geochemical phases (viz. the easily exchangeable, Mn-oxide, Fe-oxyhydroxide and residual phases) (Bau and Koschinsky, 2009; De Carlo and McMurtry, 1992; Surya Prakash et al., 2012).

Special Fe-Mn crusts, which are referred to as phosphatized crusts, are impregnated to various extents with carbonate fluorapatite and are located in the older areas of most Fe-Mn crusts (Bau et al., 1996; Jeong et al., 2000; Koschinsky et al., 1997, and references therein). Secondary phosphatized crusts show a close relationship with one or more episodes of phosphatization resulting from the expansion of the Tertiary oxygen-minimum zone (Koschinsky et al., 1997, and references therein). Geochemical and mineralogical investigations show that certain elements are depleted in phosphatized crusts compared to non-phosphatized crusts, in the following order: Si > Fe > Al > Ti ≥ Co ≥ Mn ≥ Pb; in contrast, other elements, such as Ni, Zn, Cu, Y and REE, are mostly enriched. Furthermore, one Mn oxide mineral, vernadite (δ-MnO_2), is partially recrystallized as todorokite, which is more stable under suboxic conditions (Koschinsky et al., 1997). Hence, the secondary phosphatization results for phosphatized Fe-Mn crusts are characterized by higher concentrations of P (greater than 1.3% and up to 5% in some cases), prominent positive Ce anomalies, positive La anomalies and positive Y anomalies (especially the latter, which is the most effective index for discriminating between phosphatized and non-phosphatized Fe-Mn crusts) (Bau et al., 1996; Koschinsky et al., 1997; Fig. 9).

7.2. Diagenetic Fe-Mn nodules

The Fe-Mn oxyhydroxides of diagenetic nodules form from metal ions in suboxic pore waters within soft sediment or at the sediment-water interface (Wegorzewski and Kuhn, 2014; Bau et al., 2014). Dymond et al. (1984) subdivided diagenetic nodules into two types: oxic diagenetic nodules and suboxic diagenetic nodules. The former is buried and grows in oxic sediments of the deep-sea floor, and the latter is found in hemipelagic environments where the supply of settling particles is significant enough to occasionally render a sedimentary environment suboxic or moderately reducing (Dymond et al., 1984; Takematsu et al., 1989). However, regardless of these distinctions, diagenetic nodules are closely related to hydrogenetic nodules. First, the main Mn-phase mineralogy of these nodules is todorokite, and diagenetic nodules record a much higher todorokite/vernadite ratio than hydrogenetic nodules (Calvert and Piper, 1984; Takematsu et al., 1989). Second, compared to hydrogenetic nodules, some elements are enriched or depleted in diagenetic nodules (e.g., they record increasing Mn/Fe ratios, Cu and Ni enrichment, and Co depletion) (Calvert and Piper, 1984; Roy, 1992; Takematsu et al., 1989; Wegorzewski and Kuhn, 2014). Bau et al. (2014) suggested that Ce is not quantitatively mobilized, so that Ce^{4+} remains fixed in discrete CeO_2 compounds while suboxic pore water mobilizes Mn^{2+} and REY^{3+}, producing Ce deficits in pore water and negative Ce anomalies in diagenetic nodules due to the absence of preferential oxidative scavenging of Ce from nodules. Their growth rates can be high; Dymond et al. (1984) concluded that suboxic accretion processes reach maximum rates of at least 200 mm/Ma, whereas oxic accretion is likely 10 times slower than suboxic accretion. Furthermore, hydrogenetic accretion is 100 times slower than suboxic accretion. Small Ce anomalies are likely related to high growth rates, as crusts with high growth rates can even record negative Ce anomalies (Canet et al., 2008; Kuhn et al., 1998, etc.).

Therefore, diagenetic nodules can still exhibit high total REY contents but record negative Ce anomalies due to the loss of Ce resulting from the suboxic conditions of pore water that occur during the diagenetic process. Meanwhile, because nodules that form along the sediment-water interface can scavenge REY from both bottom and interstitial water, some mixed types can be found, which record geochemical compositions and mineralogical components between those of the hydrogenetic and diagenetic end-members (Bau et al., 2014; Takematsu et al., 1989; Wegorzewski and Kuhn, 2014).

7.3. Hydrothermal Fe-Mn deposits

Hydrothermal Fe-Mn oxyhydroxide deposits precipitate from low- to medium-temperature marine hydrothermal systems. When these reducing hydrothermal fluids, which contain substantial amounts of low-valence metal ions, mix with cold seawater after exiting the seafloor, low-valence manganese and iron ions are oxidized and precipitate quickly (Mills et al., 2001; Murphy et al., 1991; Surya Prakash et al., 2012; Usui and Terashima, 1997). Hence, hydrothermal Fe-Mn deposits are mainly found in active submarine volcanoes and fault zones such as island-arc systems, volcanic chains and mid-oceanic ridges, with a depositional rate of greater than 1000 mm/Ma (Murphy et al., 1991; Surya Prakash et al., 2012; Usui and Terashima, 1997). Birnessite (7 Å manganate) is the primary mineral found in hydrothermal Fe-Mn deposits and is found abundantly in hydrothermal regions (Moorby et al., 1984; Takematsu et al., 1989; and references

therein). Due to the difference in oxidation-reduction potential between manganese and iron in oxidized marine environments, fractionation between Mn and Fe is more efficient during mixing processes that involve reducing hydrothermal fluids and oxidized seawater. For this reason, hydrothermal Fe-Mn deposits are characterized by a very wide range of Mn/Fe ratios (Moorby et al., 1984). For example, the Mn/Fe ratios of hydrothermal Fe-Mn deposits from the volcanic seamount of the Andaman Sea range from 4.0 to 126 (Surya Prakash et al., 2012), and those of the ferromanganese crusts of the TAG hydrothermal field vary from 0.002 to 3930 (Mills et al., 2001). In comparison to hydrogenetic crusts, it is difficult for hydrothermal Fe-Mn oxyhydroxides to adsorb trace elements from ambient seawater; thus, hydrothermal Fe-Mn oxyhydroxides are characterized by very low trace element concentrations (due to high sedimentary rates) and the enrichment of elements such as Ba, Li, Zn, Mo and Cd relative to hydrothermal fluids. The crystal structure of birnessite is also a vital cause of these low levels of trace elements (Post, 1999; Surya Prakash et al., 2012; and references therein). Therefore, hydrothermal Fe-Mn deposits record extremely low total REY concentrations of less than 50 ppm, and REY distribution patterns exhibit prominent negative Ce anomalies, positive Y anomalies and the relative enrichment of heavy rare earth elements, thus reflecting the distribution patterns of seawater. However, positive Eu anomalies do appear in some cases, reflecting a typical feature of hydrothermal fluids (Mills et al., 2001; Murphy et al., 1991; Olivarez and Owen, 1991; Surya Prakash et al., 2012; Fig. 9).

It is worth noting that hydrothermal Fe-Mn deposits can tend toward hydrogenetic Fe-Mn crusts along with the gradual mixing of hydrothermal fluids and seawater, which increases the total REY contents while decreasing the negative Ce and positive Y anomalies (Bau et al., 2014; Canet et al., 2008; Kuhn et al., 1998).

7.4. Discrimination between different genetic types based on REY

Based on the geochemical relationships controlling the concentrations of rare earth elements (REY) of different genetic marine Fe-Mn oxyhydroxide deposits, Bau et al. (2014) suggested that graphs of Ce anomaly *vs.* $(Y/Ho)_{SN}$ ratio and Ce anomaly *vs.* Nd concentration can effectively discriminate between genetic types of marine Fe-Mn oxyhydroxide deposits, regardless of their diverse mineralogical compositions (Fig. 11). According to Fig. 11, the hydrogenetic Fe-Mn nodules and crusts are characterized by prominent positive Ce anomalies, negative Y anomalies ($(Y/Ho)_{SN} < 1$) and very high REY concentrations (hereinafter represented as Nd concentrations); diagenetic Fe-Mn nodules are characterized by strongly negative Ce anomalies, negative Y anomalies ($(Y/Ho)_{SN} < 1$) and relatively high REY concentrations; and hydrothermal Fe-Mn deposits record prominent negative Ce anomalies, positive Y anomalies ($(Y/Ho)_{SN} > 1$) and extremely low REY concentrations. Furthermore, there is an evolutionary tendency toward hydrogenetic Fe-Mn crusts from hydrothermal Fe-Mn deposits due to the partial absorption of REY, and the oxidative scavenging of Ce and the preferential sorption of Ho relative to Y occur when Fe-Mn oxide surfaces are exposed to seawater (Fig. 11).

8. Comparative analyses

8.1. Comparison between Datangpo-type Mn ores and hydrogenetic Fe-Mn crusts/nodules

8.1.1. Similarities between Datangpo-type Mn ores and hydrogenetic Fe-Mn crusts/nodules

Based on their REY contents, Datangpo-type manganese ores are similar to hydrogenetic Fe-Mn crusts and nodules but are different than hydrothermal Fe-Mn deposits and diagenetic Fe-Mn nodules, due to their prominent positive Ce anomalies and relatively higher total REY concentrations. Similarly, on the $(Ce/Ce^*)_{SN}$ *vs.* $(Y/Ho)_{SN}$ concentration diagram (Fig. 11), manganese ores plot in the field of hydrogenetic Fe-Mn crusts and nodules. An absence of carbonate fluorapatite in manganese ores and their low P concentrations denote conditions free of secondary phosphatization. However, manganese plots in regions between the fields of hydrogenetic Fe-Mn crusts/nodules and diagenetic Fe-Mn nodules on the $(Ce/Ce^*)_{SN}$ *vs.* Nd concentration diagrams (Fig. 11), illustrating that its diagenetic modification is consistent with the results listed above.

8.1.2. Differences between Datangpo-type Mn ores and hydrogenetic Fe-Mn crusts/nodules

Compared to hydrogenetic Fe-Mn crusts and nodules, Datangpo-type manganese ores exhibit obvious differences in terms of their types of manganese-bearing minerals, total REY concentrations, magnitudes of positive Ce anomalies, degrees of fractionation between Y and Ho, and positive Eu anomalies. The reasons for these differences are analyzed as follows.

First, the Mn/Fe ratios of the Datangpo-type manganese ores are significantly greater than those of hydrogenetic crusts and nodules. This may be related to the physicochemical conditions of oceans and the degrees of fractionation between Mn and Fe. In modern

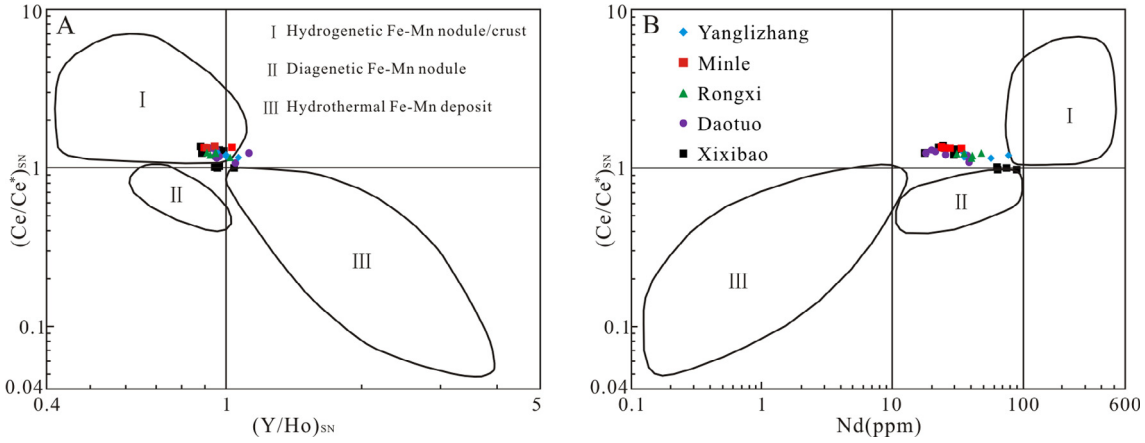

Fig. 11. (A) $(Ce/Ce^*)_{SN}$ *vs.* $(Y/Ho)_{SN}$ and (B) $(Ce/Ce^*)_{SN}$ *vs.* Nd concentration diagram of Datangpo-type manganese ores based on Bau et al., 2014. (Boundaries of fields I, II, III are demarcated based on the distributions of data presented in the referenced literature.)

marine environments, global ocean circulation results in the frequent exchange of materials between surface and bottom water columns and overall oxidation states, whereby dissolved Fe^{2+} and Mn^{2+} can be oxygenated, creating minor fractionation between Fe and Mn. Frequent exchanges of material also maintain stable ratios of Fe and Mn in seawater. Therefore, modern marine hydrogenetic crusts and nodules record smaller Mn/Fe ratios within a smaller range of values. However, the paleo-oceans of the Neoproterozoic era (ca. 1000–570 Ma) witnessed the breakup of the supercontinent Rodinia and global glaciations, which caused their physicochemical conditions to undergo complex evolutionary processes. During the tectonic stage of the rift basin, rift-related hydrothermal activities introduced substantial amounts of Fe^{2+} and Mn^{2+} into the oceans via weak metallogenesis; thereafter, metals derived from rift-related hydrothermal sources were preconcentrated in a dissolved state in stagnant, highly saline, O_2-deficient seawater beneath the ice cover, as the ice prevented any exchange of oxygen between the atmosphere and hydrosphere during glaciation (Roy, 2006). During the Fulu interglacial, temperature increases and the proliferation of algae resulted in a progressive increase in the O_2 content of surface seawater. As a result, Fe and Mn were successively oxygenated and precipitated, as iron is more easily oxygenated than manganese (Calvert and Pedersen, 1993, 1996; Glasby, 1997; Tribovillard et al., 2006). Hence, iron-bearing deposits appear in the lower Fulu Formation, whereas manganese-bearing deposits appear in the lower Datangpo Formation (Cox et al., 2013; Zhou et al., 2004), reflecting BIF and manganese deposit patterns found in the Neoproterozoic glaciogenic sequence (Cox et al., 2013; Roy, 2006). High Mn/Fe ratios are impossible to derive from hydrothermal activities, as there are no contemporaneous sediments with lower Mn/Fe ratios, although hydrothermal Fe-Mn deposits have higher Mn/Fe ratios. Similarly, diagenetic processes barely increase Mn/Fe ratios, as both Mn and Fe are dissolved and then captured in authigenic solid solutions such as Mn carbonate and pyrite in anoxic pore water, thus reflecting different conditions than the suboxic conditions of diagenetic nodules. Consequently, the greater fractionation of Mn from Fe in the Datangpo-type manganese ores is mainly caused by the evolution of the paleo-ocean over time rather than over space, and it is not correct or reasonable to identify hydrothermal origins based on Fe-Mn-(Cu + Ni + Co) × 10 ternary plots.

Second, Datangpo-type manganese ores record lower total REY concentrations, smaller positive Ce anomalies and unobvious fractionation between Y and Ho. These differences may be attributable to the following factors. (1) Relatively faster sedimentary rates. Studies show that the magnitudes of Ce anomalies in hydrogenetic crusts are closely related to crustal growth rates (Bau et al., 2014). Fe-Mn crusts with very high growth rates may record smaller positive Ce anomalies or even negative Ce anomalies in some cases. For example, Fe-Mn crusts collected from the Green Rock Hill and East Side Hill sites are characteristically hydrogenetic, due to the presence of dominant vernadite minerals, Mn/Fe ratios of approximately 0.7 and total REY concentrations of more than 1000 ppm. However, their negative Ce anomalies yield low $(Ce/Pr)_{SN}$ ratios ranging between 0.45 and 0.68 due to their high growth rates (averaging 24 mm/Ma and 23 mm/Ma, respectively, Kuhn et al., 1998). The Fe-Mn crusts of the Rivera Plate (on the western margin of Mexico) record an absence of positive cerium anomalies, complementing their high growth rates (Canet et al., 2008). Relatively faster sedimentary rates can produce lower total REY concentrations and unobvious fractionation between Y and Ho, as the exchange equilibrium between metal oxide particles and seawater cannot increase if the reaction time is not sufficient, which is particularly evident in hydrothermal deposits. (2) Relatively shallower water columns. Datangpo-type manganese ores exist in epicontinental semi-limited shallow basin sedimentary environments at depths of much less than those of modern hemi-pelagic and pelagic environments. Shorter particle residence times in water columns result in relatively weak REY partitioning. (3) Hydrothermal activity. High growth rates mainly occur in some hydrogenetic crusts due to hydrothermal activity (Canet et al., 2008; Kuhn et al., 1998). The REY distribution patterns of hydrothermal deposits are opposite those of hydrogenetic crusts. Hence, hydrothermal activity can offset total REY concentrations, as well as the magnitudes of positive Ce anomalies and negative Y anomalies. (4) Relatively higher Mn/Fe ratios. The REY absorption capacities of Mn oxide and Fe-oxyhydroxide phases are not identical. In comparing the partition coefficients of single components of Mn oxides and Fe-oxyhydroxides, Bau and Koschinsky (2009) found substantial variation in the extent of oxidative scavenging for Ce between Mn oxide and Fe-oxyhydroxide phases, but they found that Y absorption is more closely associated with Mn oxides than with Fe-oxyhydroxides, according to the results of a sequential leaching procedure performed on hydrogenetic Fe-Mn crusts from the Central Pacific. Consequently, the size of a negative Y anomaly becomes small or negligible when the Mn content is much greater than that of Fe. Similarly, Surya Prakash et al. (2012) reported that the REY distribution patterns of Fe-oxyhydroxide phases record more obvious positive Ce anomalies and negative Y anomalies than do those of Mn oxides, based on the results of a similar sequential leaching procedure performed on hydrogenetic Fe-Mn crusts from seamounts of the Andaman Sea. (5) Organic matter. The contributions of organic matter are not negligible, and Pi et al. (2013) suggest that the REY derived from microorganism enrichment yield seawater-like patterns and are characterized by distribution patterns featuring evident negative Ce anomalies and positive Y anomalies. Therefore, some of the positive Ce anomalies and negative Y anomalies in Mn oxides may be offset by organic matter.

For these reasons, factors (1), (2) and (5) should cause the significant decrease of positive Ce anomalies, negative Y anomalies and total REY concentrations, although the sedimentary rate of the Datangpo-type manganese ores has not been measured. Under faster sedimentary rates, Mn-oxyhydroxides may be precipitated through the rapid accumulation of unconsolidated sediments rather than through the growth of crusts or nodules. Thus, by taking these above issues into consideration, the causes of the negative Ce anomalies may be determined. However, this is likely not the case, because another factor can increase the size of the positive Ce anomaly: the presence of high Ce concentrations in the water column prior to manganese deposition. Mn and Ce should be dominated by a dissolved divalent state in the anoxic bottom waters of O_2-stratified restricted basins and should thus be present in much higher background concentrations, as Mn and Ce exhibit similar geochemical behaviors in anoxic environments (Loges et al., 2012; Moffett, 1990). Similarly, in modern anoxic basins (e.g., the Black Sea), Ce is enriched in lower anoxic water columns and bottom seawater exhibits a very weak negative or even slightly positive Ce anomaly (Holser, 1997, and references therein). In addition, there is a positive correlation between the size of the positive Ce anomaly and Mn concentration. This is consistent with the principle that positive Ce anomalies are limited by Mn oxide levels and not by Ce in water columns, thus demonstrating that Ce content sufficiently facilitates absorption by Mn oxides.

Comparisons of the similarities and differences between modern marine Fe-Mn sediments and Datangpo-type Mn ores on the basis of REY demonstrates that the REY concentrations of Datangpo-type Mn ores are much higher than those of hydrothermal Fe-Mn sediments. Additionally, the presence of obviously positive Ce anomalies excludes the hydrothermal genesis of Datangpo-type Mn ores. The positive Ce anomalies of Datangpo-type Mn ores are clearly different than the negative Ce anomalies of diagenetic

nodules, but similar to those of the hydrogenetic crusts and nodules, which are characterized by high REY contents and positive Ce anomalies. This illustrates that the sedimentary processes of the Datangpo-type Mn ores are similar to those of the modern ocean hydrogenetic crusts and nodules and reflects that Mn precipitated as Mn-oxyhydroxides under oxic conditions.

However, compared to hydrogenetic Fe-Mn crusts and nodules, Datangpo-type manganese ores exhibit obvious differences in terms of their types of manganese-bearing minerals, Mn/Fe values, total concentrations of REY, magnitudes of positive Ce anomalies, degrees of fractionation between Y and Ho, and positive Eu anomalies. Datangpo-type manganese ores have lower contents of REY, smaller magnitudes of positive Ce anomalies, and unobvious fractionation between Y and Ho, which result from faster sedimentary rates, shallower basin water columns and organic matter.

Consequently, compared to hydrogenetic Fe-Mn crusts and nodules, Datangpo-type manganese ores precipitated as Mn-oxyhydroxides via faster sedimentary rates under oxic conditions within shallower basin water columns.

The positive Eu anomalies of the Datangpo-type manganese ores, which represent another difference from the hydrogenetic Fe-Mn crusts and nodules, resulted from the degradation of organic matter after oxide deposition. In an early diagenetic stage, Mn-oxyhydroxides were reduced and transformed into rhodochrosite, because the alkaline reducing conditions were stronger than those of the diagenetic Fe-Mn nodules. At the same time, Eu^{2+} entered the carbonate mineral lattice, resulting in positive Eu anomalies.

8.2. Comparison between Datangpo-type Mn ores and country rocks

The differences in the characteristics of the rare earth elements between the Datangpo-type Mn ores and country rocks (black shales) could be attributed to multiple factors. In addition to differences in the origins of REY, factors such as the redox conditions of the formation environment, sedimentary rates, the production rate of organic matter and organic burial capacity could have produced the PAAS-normalized distribution patterns of rare earth elements, Ce anomalies and Eu anomalies of the Mn ores and black shales.

The REY of the Mn ores are mainly derived from the input of terrigenous detrital materials, sorption by Mn-oxyhydroxides and microorganism enrichment, whereas the REY of the black shales are derived from the input of terrigenous detrital materials and organic sorption.

Wright (1987) proposed Ce_{anom} ($lg[3Ce_n/(2\ La_n + Nd_n)]$) = −0.1 as a redox interface, in which $Ce_{anom} > -0.1$ represents reducing conditions while $Ce_{anom} < -0.1$ represents oxic conditions. The average Ce_{anom} of the country rocks is 0.015 ($-0.008 \sim 0.58$), which represents a reducing sedimentary environment. However, geochemical analysis of the Datangpo-type Mn ores indicates that the Mn ores hosted in the first member of Datangpo formation formed under oxic conditions, therefore, there is an incompatibility between the sedimentary environments of the Mn ores and the country rocks.

The relatively weak fractionation of Y and Ho and the smaller magnitudes of the positive Ce anomalies in the Datangpo-type Mn ores indicate that they may have featured relatively quick sedimentary rates. That is, strong hydrodynamic conditions may have existed during the precipitation of Mn ores, rather than a lentic environment, as was proposed by previous scholars. This was confirmed by the structure and construction of the Mn ores. In contrast, the stronger Y/Ho fractionation of the country rocks reflects the slower sedimentary rates of the black shales within a lentic environment, which was confirmed by their horizontally-laminated beds.

The PAAS-normalized distribution patterns of the rare earth elements (REY_{SN}) of the manganese ores are characterized by the pronounced enrichment of middle rare earth elements (MREEs), producing a "hat-shaped" REY plot, which can also be found in the PAAS-normalized distribution patterns of the rare earth elements of rocks and minerals from other geological eras. These include petrologen hosted in the Early Cambrian black shales of Guizhou province (Pi et al., 2013), phosphorite hosted in the lower Cambrian Series of Yunnan province (Shields and Stille, 2001), phosphatic nodules hosted in the Niutitang Formation of Western Hunan (Zhu et al., 2014), phosphatic rocks hosted in Neoproterozoic Ediacaran Doushantuo Formation of Western Hubei (Xin et al., 2015), and some fossil organisms (Wright et al., 1987). The formations of all of these rocks and minerals are related to organic matter. The PAAS-normalized distribution patterns of the rare earth elements (REY_{SN}) of manganese ores, which are similar to those of these rocks and minerals, indicates that this "hat shape" may be related to the degradation of organic matter in the early diagenetic stage. The PAAS-normalized distribution patterns of the rare earth elements of the black shales, which yield "flat-shaped" REY plots, are similar to those of black argillaceous rock from different geological eras (Fan et al., 2004). These PAAS-normalized distribution patterns of rare earth elements are typically caused by terrigenous clastic material (Pi et al., 2013).

The positive Ce anomalies of Mn ores are closely related to the oxidative sorption of manganese. It is believed that Mn precipitates in oxidized water columns as Mn-oxides or Mn-oxyhydroxides, absorbing abundant Ce along with organic granules to produce positive Ce anomalies. The weakly positive Eu anomalies of Mn ores may be caused by the degradation of organic matter under alkaline reduction conditions after burial. Eu^{2+} was formed through the reduction of Eu^{3+} in reducing alkaline pore waters, which then entered the crystal lattice of carbonate minerals, causing Eu enrichment and producing positive Eu anomalies. Generally, sediments formed under anoxic conditions record negative Ce anomalies; no Ce anomalies are seen in these country rocks, which may be related to organic sorption.

Furthermore, the P_2O_5 concentrations of manganese ores and black shale samples may be related to sedimentary conditions. Table 2 shows that manganese ores contain more P_2O_5 relative to black shales, which may be related to their faster sedimentary rates. Studies have shown that the concentrations of P in sediments or sedimentary rocks have important indicative significance for organic matter production rates in the euphotic zone through two different processes. (1) Under anoxic conditions, P formed by the degradation of organic matter was released through sediments into water, thereafter shifting to a euphotic zone due to the multiplication of phytoplankton. That is, there was an efficient geochemical phosphorus cycle between sediments and water volume, where minimal organic P broke away from the cycle and was preserved in sediments. Under this phosphorus cycle, high organic matter production rates and P enrichment were not recorded in sediments, thus resulting in slow deposition within a lentic environment. (2) Under certain conditions, P formed by the degradation of organic matter was released into pore water, not into the overlying water. Phosphorous-bearing authigenic minerals, such as apatite (Tribovillard et al., 2006), were formed when the P content of pore water reached a high enough concentration, which resulted from the rapid burial of organic matter. The black shales, which formed under anoxic conditions, had lower P_2O_5 contents, which correspond to the first condition. In contrast, the Mn ores, which formed under oxic conditions, had higher P_2O_5 contents, which correspond to the second condition. Therefore, differences in the P_2O_5 concentrations of the black shales and Mn ores may indicate that the black shales were formed by slower sedimentary rates within a lentic environment, where a geochemical

Table 4
Contrasting characteristics between Datangpo-type manganese deposits and typical manganese deposits around the world.

Deposit name	Deposit locality	Manganese minerals	∑REE (PPm)	$(Ce/Ce^*)_{SN}$	$(Eu/Eu^*)_{SN}$	$(Y/Y^*)_{SN}$	Reference
Datangpo-type Manganese Deposits	Northeastern of Guizhou province and adjacent areas, China	Rhodochrosite Calcium- Rhodochrosite	222.67	1.25	1.15	0.89	This study
Xialei Manganese Deposits	Guangxi Zhuang Autonomos Region, China	Rhodochrosite, Calcium- Rhodochrosite,	142.76	1.11	1.14	0.89	Qin et al. (2010)
Zunyi Manganese Deposits	Guizhou province, China	Rhodochrosite, Calcium-Rhodochrosite, Calcimangite	517.26	0.32	0.96	2.09	Liu et al. (2015)
Orissa Manganese Deposits	Orissa, East India	Cryptomelane, hollandite, pyrolusite	284.12	0.2	1.33	0.81	Moriyama et al. (2008)
Maden complex Ferromanganese Deposits	Elazığ-Malatya region, Eastern Turkey	Braunite, Bixbyite, Jacobsite, Pyrolusite, Manganite, Psilomelane	517.85	0.15	1.14	0.94	Ahmet et al. (2014)
Kalahari Manganese Deposit	Northern Cape Province of South Africa	Braunite	19.15	0.59	1.26		Chetty and Gutzmer (2012)

P-cycle existed between sediments and the water volume, whereas the Mn ores were formed by quicker sedimentary rates and the geochemical P-cycle between sediments and water volume was interdicted by the rapid burial of terrigenous materials and organic matter.

8.3. Comparison between Datangpo-type Mn ores and manganese deposits around the world

8.3.1. Characteristics of typical manganese deposits around the world (Table 4)

1) The Xialei Manganese Deposit is one of the super-large mineral deposits in Asia. Its reserves of Mn ores contain over 100 million tons. Manganese ore bodies are hosted in the Wuzhishan Formation of the Devonian system. The main minerals are Mn-carbonates; in the middle-bottom part of the ore bodies are rhodonite and Fe-Mn serpentine, which are related to hydrothermal activity. The country rocks are mainly composed of mud calcareous siliceous rocks and siliceous limestone. Manganese ores have weakly positive Ce anomalies, Eu anomalies and negative Y anomalies, without fractionation between LREE and HREE. Mn-carbonates precipitated from marine sedimentary environments through normal sedimentation, along with the injection and supplement of deep hydrothermal fluids and biological activity (Qin et al., 2010).
2) The Zunyi Manganese Deposit is a large deposit. Its ore bodies are hosted in the Longtan Formation of the Permian system, and the Mn minerals of the ore bodies are mainly Mn-carbonates. The bottom country rocks are sage-green clay rocks, and the top country rocks comprise gray clay rocks and siliceous limestone. Manganese ores are HREE-enriched Mn deposits with very high ∑REE, which record evident negative Ce anomalies and positive Y anomalies without Eu anomalies. Hydrothermal exhalative sedimentation is the main genesis of Mn ores, accompanied by normal chemical sedimentation (Liu et al., 2015).
3) The Orissa Manganese Deposits are hosted in the Upper Shale Formation of the Late Archean Iron Ore Group. Manganese and ferromanganese ores are composed of cryptomelane, hollandite and pyrolusite, while the country rocks are mainly composed of shale and dolomite. These rocks record wide variations in ∑REE as well as HREE enrichment, obvious negative Ce anomalies, stronger positive Eu anomalies and weak negative Y anomalies. These REE signatures suggest that the manganese and ferromanganese ores were formed by iron and manganese precipitation from a submarine hydrothermal solution under oxic conditions that occurred as the result of mixing with oxic seawater (Moriyama et al., 2008).
4) The Maden complex ferromanganese deposits are hosted in the Middle Eocene Melafan Formation. Their Mn-mineral assemblages are composed of manganese oxide minerals. The surrounding rocks are mainly mudstone and spilitic basalt. The Mn ores have very high REE concentrations with no fractionation between HREE and LREE, remarkably negative Ce anomalies, weakly positive Eu anomalies and hardly any Y anomalies. These REE characteristics suggest that the Maden complex deposits were formed by hydrothermal processes (Ahmet et al., 2014).
5) The Kalahari Manganese deposit, which is the largest land-based manganese deposit in the world, is hosted in the Paleoproterozoic Hotazel Formation and is a hydrothermal manganese deposit surrounded by banded iron formations (BIF) and hematite lutite (Chetty and Gutzmer, 2012). Braunite is the main Mn-mineral in the least altered Mn ores of the Northern Kalahari manganese deposit. The REE concentrations of this Mn ore are very low (only 19.15 ppm), which slightly exceed the ∑REE of protolith (18.87 ppm). The Mn ores record negative Ce anomalies, positive Eu anomalies, and HREE enrichment.

8.3.2. Contrasts in the characteristics of Datangpo-type manganese ores and typical manganese deposits around the world

Based on the characteristics of the ore deposits discussed above, there are obvious differences between the Datangpo-type manganese ores and the Zunyi Mn ores, Orissa Mn ores, Maden Mn ores and Kalahari Mn ores in terms of their mineral assemblages and REE geochemical compositions. Overall, the common characteristics of these deposits are negative Ce anomalies and HREE enrichment caused by hydrothermal activity.

The REE geochemical compositions of the Datangpo-type manganese ores are most similar to those of the Xialei manganese ores. Both of these ores have positive Ce anomalies, weak positive Eu anomalies, weak negative Y anomalies, and no fractionation between HREE and LHEE. Additionally, both of their mineral assemblages are mainly rhodochrosite and calcium rhodochrosite. The deposition of the Xialei manganese ores is mainly that of normal marine sedimentation.

Based on these differences, the Datangpo-type manganese ores are evidently different than hydrothermal manganese ores, but show similarities to hydrogenetic manganese ores. These features suggest that the sedimentary genesis of the Datangpo-type manganese ores is mainly that of normal marine sediment.

9. Conclusions

1) The PAAS-normalized distribution patterns of the rare earth elements of the Datangpo-type manganese ores are characterized by the pronounced enrichment of middle rare earth elements, producing a so-called "hat-shaped" REY plot, as well as the presence of prominent positive Ce anomalies, weak to strong positive Eu anomalies, and negligible negative Y anomalies. These REY geochemical characteristics, which are different than those of the country rocks, record the processes and features of sedimentation-diagenesis. Manganese was precipitated as Mn-oxyhydroxide particles in oxidized water columns with the sorption of a certain amount of rare earth elements, thereafter transforming from Mn-oxyhydroxides to rhodochrosite and redistributing REY in reducing alkaline pore-water through an early diagenetic stage.
2) Compared to modern marine Fe-Mn oxyhydroxide precipitates, Datangpo-type manganese ores are similar to hydrogenetic crusts and nodules, both of which record positive Ce anomalies and relatively higher levels of total REY content, but are different than diagenetic nodules and hydrothermal deposits, which can be confirmed by comparative analysis between Datangpo-type manganese ores and typical Mn deposits of the world.
3) Compared to hydrogenetic crusts and nodules, Datangpo-type manganese ores show smaller magnitudes of positive Ce anomalies, lower levels of total REY contents, minor fractionation between Y and Ho, and weak to strong positive Eu anomalies. These factors were caused by quicker sedimentary rates under oxic, shallower water columns, after which pore water became strongly reducing and alkaline due to the degradation of organic matter in an early diagenetic stage.

Acknowledgments

This work was supported through the National Basic Research Program of China (2014CB440906) and through the 12th Five Year Plan Project of the State Key Laboratory of Ore Deposit Geochemistry at the Chinese Academy of Science (SKLODG-Zy125-08). We appreciate the input of advanced experimentalist Jing Hu, Guang Pin Bao, Yan Huang in facilitating the geochemical element analyses and determinations. A gratefully acknowledge scanning electron microscopy guidance provided by Professor Shi Rong Liu and Dr. Yang Tang.

References

Ahmet, Ş.M., Bayram, T.M., Nevin, Ö.T., Fuat, Y., Mustafa, K.M., 2014. Geology and geochemistry of Middle Eocene Maden complex ferromanganese deposits from the Elazığ-Malatya region, eastern Turkey. Ore Geol. Rev. 56, 352–372.

Alibo, D.S., Nozaki, Y., 1999. Rare earth elements in seawater: particle association, shale-normalization, and Ce oxidation. Geochim. Cosmochim. Acta 63 (3–4), 363–372.

An, Z.Z., Zhang, R.B., Chen, J.C., Qin, Y., Wu, G.W., Peng, Q.Y., Zheng, C., Zhang, F.F., Zhu, X.K., Wang, H.B., 2014. Geological and geochemical characteristics of Daotuo super large manganese ore deposit in Songtao County of Guizhou Province: constraints formation mechanism of Mn-carbonate ores. Miner. Deposits 33 (4), 870–884 (in Chinese with English abstract).

Bau, M., Dulski, P., 1995. Comparative study of yttrium and rare-earth element behaviours in fluorine-rich hydrothermal fluids. Contrib. Miner. Petrol. 119 (2–3), 213–223.

Bau, M., Dulski, P., 1996. Distribution of yttrium and rare-earth elements in the Penge and Kuruman iron-formations, Transvaal Supergroup, South Africa. Precambr. Res. 79 (1–2), 37–55.

Bau, M., Dulski, P., 1999. Comparing yttrium and rare earths in hydrothermal fluids from the Mid-Atlantic Ridge: implications for Y and REE behaviour during near-vent mixing and for the Y/Ho ratio of Proterozoic seawater. Chem. Geol. 155 (1–2), 77–90.

Bau, M., Koschinsky, A., 2009. Oxidative scavenging of cerium on hydrous Fe oxide: evidence from the distribution of rare earth elements and yttrium between Fe oxides and Mn oxides in hydrogenetic ferromanganese crusts. Geochem. J. 43 (1), 37–47.

Bau, M., Koschinsky, A., Dulski, P., Hein, J.R., 1996. Comparison of the partitioning behaviours of yttrium, rare earth elements, and titanium between hydrogenetic marine ferromanganese crusts and seawater. Geochim. Cosmochim. Acta 60 (10), 1709–1725.

Bau, M., Möller, P., Dulski, P., 1997. Yttrium and lanthanides in eastern Mediterranean seawater and their fractionation during redox-cycling. Mar. Chem. 56 (1–2), 123–131.

Bau, M., Schmidt, K., Koschinsky, A., Hein, J., Kuhn, T., Usui, A., 2014. Discriminating between different genetic types of marine ferro-manganese crusts and nodules based on rare earth elements and yttrium. Chem. Geol. 381, 1–9.

Calvert, S.E., Pedersen, T.F., 1993. Geochemistry of Recent oxic and anoxic marine sediments: implications for the geological record. Mar. Geol. 113 (1–2), 67–88.

Calvert, S.E., Pedersen, T.F., 1996. Sedimentary geochemistry of manganese: implications for the environment of formation of manganiferous black shales. Econ. Geol. 91 (1), 36–47.

Calvert, S.E., Piper, D.Z., 1984. Geochemistry of ferromanganese nodules from DOMES site a, Northern Equatorial Pacific: multiple diagenetic metal sources in the deep sea. Geochim. Cosmochim. Acta 48 (10), 1913–1928.

Canet, C., Prol-Ledesma, R.M., Bandy, W.L., Schaaf, P., Linares, C., Camprubí, A., Tauler, E., Mortera-Gutiérrez, C., 2008. Mineralogical and geochemical constraints on the origin of ferromanganese crusts from the Rivera Plate (western margin of Mexico). Mar. Geol. 251 (1–2), 47–59.

Chetty, D., Gutzmer, J., 2012. REE redistribution during hydrothermal alteration of ore of the Kalahari Manganese Deposit. Ore Geol. Rev. 47, 126–135.

Chisonga, B.C., Gutzmer, J., Beukes, N.J., Huizenga, J.M., 2012. Nature and origin of the protolith succession to the Paleoproterozoic Serra do Navio manganese deposit, Amapa Province, Brazil. Ore Geol. Rev. 47, 59–76.

Cox, G.M., Halverson, G.P., Minarik, W.G., Le Heron, D.P., Macdonald, F.A., Bellefroid, E.J., Strauss, J.V., 2013. Neoproterozoic iron formation: an evaluation of its temporal, environmental and tectonic significance. Chem. Geol. 362, 232–249.

Cui, Y.C., Liu, J.H., Ren, X.W., Shi, X.F., 2009. Geochemistry of rare earth elements in cobalt-rich crusts from the Mid-Pacific M seamount. J. Rare Earths 27 (1), 169–176.

Dai, C.G., Chen, J.S., Lu, D.B., Ma, H.Z., Wang, X.H., 2010. Wuling orogeny in eastern Guizhou and its adjacent region and its geological significance. J. Geomech. 16 (1), 78–84 (in Chinese with English abstract).

De Carlo, E.H., McMurthy, G.M., Kim, K.H., 1987. Geochemistry of ferromanganese crusts from the Hawaiian Archipelago—I. Northern survey areas. Deep Sea Res. Part I: Oceanogr. Res. Papers 34 (3), 441–467.

De Carlo, E.H., McMurtry, G.M., 1992. Rare-earth element geochemistry of ferromanganese crusts from the Hawaiian Archipelago, central Pacific. Chem. Geol. 95 (3–4), 235–250.

De Carlo, E.H., Wen, X.Y., Irving, M., 1997. The influence of redox reactions on the uptake of dissolved Ce by suspended Fe and Mn oxide particles. Aquat. Geochem. 3 (4), 357–389.

Dobrzinski, N., Bahlburg, H., 2007. Sedimentology and environmental significance of the Cryogenian successions of the Yangtze Platform, South China block. Palaeogeogr. Palaeoclimatol. Palaeoecol. 254 (1–2), 100–122.

Douville, E., Bienvenu, P., Charlou, J.L., Donval, J.P., Fouquet, Y., Appriou, P., Gamo, T., 1999. Yttrium and rare earth elements in fluids from various deep-sea hydrothermal systems. Geochim. Cosmochim. Acta 63 (5), 627–643.

Dymond, J., Lyle, M., Finney, B., Piper, D.Z., Murphy, K., Conard, R., Pisias, N., 1984. Ferromanganese nodules from MANOP Sites H, S, and R—Control of mineralogical and chemical composition by multiple accretionary processes. Geochim. Cosmochim. Acta 48 (5), 931–949.

Fan, D.L., Yang, P.J., 1999. Introduction to and classification of manganese deposits of China. Ore Geol. Rev. 15 (1–3), 1–13.

Fan, D.L., Zhang, T., Ye, J., 2004. Black Rock Series and Associated Deposits in China. Science Pub. House, Beijing, pp. 1–236 (in Chinese).

Gao, L.Z., Lu, J.P., Ding, X.Z., Wang, H.R., Liu, Y.X., Li, J., 2013. Zircon U-Pb dating of Neoproterozoic tuff in South Gaungxi and its implications for stratigraphic correlation. Geol. China 40 (5), 1443–1452 (in Chinese with English abstract).

Glasby, G.P., 1997. Fractionation of manganese from iron in Archaean and Proterozoic sedimentary ores. Geological Society, London, Special Publications 119 (1), 29–42.

Halbach, P., Scherhag, C., Hebisch, U., Marchig, V., 1981. Geochemical and mineralogical control of different genetic types of deep-sea nodules from the Pacific Ocean. Miner. Deposita 16 (1), 59–84.

He, Z.W., Yang, R.D., Gao, J.B., Cheng, W., Zhang, R.B., Zhang, P.Y., 2013. Sedimentary geochemical characteristics of manganese deposits in Xixibao, Songtao County, Guizhou Province. Geochimica 42 (6), 576–588 (in Chinese with English abstract).

Holser, W.T., 1997. Evaluation of the application of rare-earth elements to paleoceanography. Palaeogeogr. Palaeoclimatol. Palaeoecol. 132 (1–4), 309–323.

Hou, Z.L., Xue, Y.Z., Huang, J.S., Zhu, K.J., Lin, Y.H., Liu, H.J., Yao, J.Q., Zhu, K.J., 1997. Manganese Ore Deposits Around Yangtze Platform. Metallurgical Industry Press, Beijing, pp. 1–350 (in Chinese).

Jeong, K.S., Jung, H.S., Kang, J.K., Morgan, C.L., Hein, J.R., 2000. Formation of ferromanganese crusts on northwest intertropical Pacific seamounts: electron photomicrography and microprobe chemistry. Mar. Geol. 162 (2–4), 541–559.

Jiang, G.Q., Sohl, L.E., Christie-Blick, N., 2003. Neoproterozoic stratigraphic comparison of the Lesser Himalaya (India) and Yangtze block (south China): paleogeographic implications. Geology 31 (10), 917–920.
Kidder, D.L., Krishnaswamy, R., Mapes, R.H., 2003. Elemental mobility in phosphatic shales during concretion growth and implications for provenance analysis. Chem. Geol. 198 (3–4), 335–353.
Koeppenkastrop, D., De Carlo, E.H., 1992. Sorption of rare-earth elements from seawater onto synthetic mineral Particles-An experimental approach. Chem. Geol. 95 (3–4), 251–263.
Koeppenkastrop, D., De Carlo, E.H., 1993. Uptake of rare earth elements from solution by metal oxides. Environ. Sci. Technol. 27 (9), 1796–1802.
Koschinsky, A., Hein, J.R., 2003. Uptake of elements from seawater by ferromanganese crusts: solid-phase associations and seawater speciation. Mar. Geol. 198 (3–4), 331–351.
Koschinsky, A., Stascheit, A., Bau, M., Halbach, P., 1997. Effects of phosphatization on the geochemical and mineralogical composition of marine ferromanganese crusts. Geochim. Cosmochim. Acta 61 (19), 4079–4094.
Kuhn, T., Bau, M., Blum, N., Halbach, P., 1998. Origin of negative Ce anomalies in mixed hydrothermal–hydrogenetic Fe–Mn crusts from the Central Indian Ridge. Earth Planet. Sci. Lett. 163 (1–4), 207–220.
Kunzendorf, H., Glasby, G.P., Stoffers, P., Plüger, W.L., 1993. The distribution of rare earth and minor elements in manganese nodules, micronodules and sediments along an east-west transect in the southern Pacific. Lithos 30 (1), 45–56.
Li, X.H., Li, W.X., Li, Z.X., Lo, C.H., Wang, J., Ye, M.F., Yang, Y.H., 2009. Amalgamation between the Yangtze and Cathaysia Blocks in South China: constraints from SHRIMP U-Pb zircon ages, geochemistry and Nd–Hf isotopes of the Shuangxiwu volcanic rocks. Precambr. Res. 174 (1–2), 117–128.
Lin, S.J., Lu, D.B., Xiao, J.F., Xiong, X.H., Li, Y.T., 2013. Stratigraphy of the Nanhuan system in Guizhou province. J. Stratigr. 37 (4), 542–557 (in Chinese with English abstract).
Liu, B.J., Xu, X.S., Xu, Q., Pan, X.N., Huang, H.Q., 1993. Sedimentary Crustal Evolution and Mineralization of Palaeocontinent in South China. Science Pub. House, Beijing, pp. 1–236 (in Chinese).
Liu, J.S., 1994. Early Sinian sedimentary formations, turbidite and manganese ore genesis. Geotectonica Metallogenia 18 (2), 174–182 (in Chinese with English abstract).
Liu, X.F., Hu, Z.R., Zeng, L.X., Zheng, G.X., Wang, C.Y., 1983. Origin and characteristics of sedimentary facies of Sinian manganese deposits in Guizhou. Acta Sedimentol. Sin. 1 (4), 106–118 (in Chinese with English abstract).
Liu, X.F., Wang, Q.S., Gao, X.J., 1989. Guizhou Manganese Geology. Guizhou People Pub. House, Guiyang, pp. 1–194 (in Chinese).
Liu, Z.C., Wang, C., Zhang, Y.G., Fang, B., Chen, D., Wei, Z.Q., Cui, Z.Q., 2015. Geochemistry and Ore Genesis of Zunyi Mn Deposit, Guizhou Province, China. Acta Mineral. Sin. 35 (4), 481–488 (in Chinese with English abstract).
Loges, A., Wagner, T., Barth, M., Bau, M., Göb, S., Markl, G., 2012. Negative Ce anomalies in Mn oxides: the role of Ce^{4+} mobility during water–mineral interaction. Geochim. Cosmochim. Acta 86, 296–317.
Lu, D.B., Xiao, J.F., Lin, S.J., Liu, A.M., Mou, S.Y., Chen, R., Yi, C.X., Wang, X.L., 2010. The Nanhuaan section at Lijiapo Village, Congjiang County, Guizhou Province in Hunan -Guizhou -Guangxi adjacent region, China–a good section with sedimentary record in Nanhuaan Large Glaciation age. Geol. Bull. China 29 (8), 1143–1151 (in Chinese with English abstract).
Maceae, N.D., Nesbitt, H.W., Kronberg, B.I., 1992. Elemental mobility in phosphatic shales during concretion growth and implications for provenance analysis. Elemental mobility in phosphatic shales during concretion growth and implications for provenance analysis, 109(3-4), 585–591.
Martinez-Ruiz, F., Ortega-Huertas, M., Palomo, I., 1999. Positive Eu anomaly development during diagenesis of the K/T boundary ejecta layer in the Agost section (SE Spain): implications for trace-element remobilization. Terra Nova 11 (6), 290–296.
Mills, R.A., Wells, D.M., Roberts, S., 2001. Genesis of ferromanganese crusts from the TAG hydrothermal field. Chem. Geol. 176 (1–4), 283–293.
Moffett, J.W., 1990. Microbially mediated cerium oxidation in sea water. Nature 345 (6274), 421–423.
Moffett, J.W., 1994. A radiotracer study of cerium and manganese uptake onto suspended particles in Chesapeake Bay. Geochim. Cosmochim. Acta 58 (2), 695–703.
Moorby, S.A., Cronan, D.S., Glasby, G.P., 1984. Geochemistry of hydrothermal Mn-oxide deposits from the S.W. Pacific island arc. Geochim. Cosmochim. Acta 48 (3), 433–441.
Moriyama, T., Panigrahi, M.K., Pandit, D., Watanabe, Y., 2008. Rare earth element enrichment in Late Archean manganese deposits from the Iron Ore Group, East India. Resour. Geol. 58 (4), 402–413.
Murphy, E., McMurtry, G.M., Kim, K.H., De Carlo, E.H., 1991. Geochemistry and geochronology of a hydrothermal ferromanganese deposit from the North Fiji Basin. Mar. Geol. 98 (2–4), 297–312.
Nyame, F.K., Beukes, N.J., Kase, K., Yamamoto, M., 2003. Compositional variations in manganese carbonate micronodules from the Lower Proterozoic Nsuta deposit, Ghana: product of authigenic precipitation or post-formational diagenesis? Sed. Geol. 154 (3–4), 159–175.
Ohta, A., Kawabe, I., 2001. REE(III) adsorption onto Mn dioxide (δ-MnO2) and Fe oxyhydroxide: Ce(III) oxidation by δ-MnO2. Geochim. Cosmochim. Acta 65 (5), 695–703.
Okita, P.M., Maynard, J.B., Spiker, E.C., Force, E.R., 1988. Isotopic evidence for organic matter oxidation by manganese reduction in the formation of stratiform manganese carbonate ore. Geochim. Cosmochim. Acta 52 (11), 2679–2685.
Okita, P.M., Shanks III, W.C., 1992. Origin of stratiform sediment-hosted manganese carbonate ore deposits: Examples from Molango, Mexico, and TaoJiang, China. Chem. Geol. 99 (1–3), 139–163.
Olivarez, A.M., Owen, R.M., 1991. The europium anomaly of seawater: implications for fluvial versus hydrothermal REE inputs to the oceans. Chem. Geol. 92 (4), 317–328.
Pattan, J.N., Pearce, N.J.G., Mislankar, P.G., 2005. Constraints in using Cerium-anomaly of bulk sediments as an indicator of paleo bottom water redox environment: a case study from the Central Indian Ocean Basin. Chem. Geol. 221 (3–4), 260–278.
Pi, D.H., Liu, C.Q., Shields-Zhou, G.A., Jiang, S.Y., 2013. Trace and rare earth element geochemistry of black shale and kerogen in the early Cambrian Niutitang Formation in Guizhou province, South China: constraints for redox environments and origin of metal enrichments. Precambr. Res. 225, 218–229.
Polgári, M., Hein, J.R., Vigh, T., Szabó-Drubina, M., Fórizs, I., Bíró, L., Müller, A., Tóth, A.L., 2012. Microbial processes and the origin of the Úrkút manganese deposit, Hungary. Ore Geol. Rev. 47, 87–109.
Post, J.E., 1999. Manganese oxide minerals: crystal structures and economic and environmental significance. Proc. Natl. Acad. Sci. U.S.A. 96 (7), 3447–3454.
Pourret, O., Davranche, M., 2013. Rare earth element sorption onto hydrous manganese oxide: a modeling study. J. Colloid Interface Sci. 395, 18–23.
Pourret, O., Davranche, M., Gruau, G., Dia, A., 2008. New insights into cerium anomalies in organic-rich alkaline waters. Chem. Geol. 251 (1–4), 120–127.
Qin, Y., An, Z.Z., Wang, J.W., Li, D.P., 2013. The discovery and geological characteristics of the super-large sized Daotuo manganese deposits in Songtao, Guizhou. Miner. Explor. 4 (4), 345–355 (in Chinese with English abstract).
Qin, Y., Zhou, Q., Zhang, S., 2005. Elementary Properties of Manganese of Nh in the Northeastern Guizhou. Guizhou Geol. 22 (4), 246–251 (in Chinese with English abstract).
Qin, Y.K., Zhang, H.C., Yao, J.Q., 2010. Geochemical Characteristics and Geological Implication of the Xialei Manganese Deposit, Daxin County, Guangxi. Geol. Rev. 56 (5), 664–672 (in Chinese with English abstract).
Roy, S., 1992. Environments and processes of manganese deposition. Econ. Geol. 87 (5), 1218–1236.
Roy, S., 2006. Sedimentary manganese metallogenesis in response to the evolution of the Earth system. Earth Sci. Rev. 77 (4), 273–305.
Sabatino, N., Neri, R., Bellanca, A., Jenkyns, H.C., Masetti, D., Scopelliti, G., 2011. Petrography and high-resolution geochemical records of Lower Jurassic manganese-rich deposits from Monte Mangart, Julian Alps. Palaeogeogr. Palaeoclimatol. Palaeoecol. 299 (1–2), 97–109.
Shields, G., Stille, P., 2001. Diagenetic constraints on the use of cerium anomalies as palaeoseawater redox proxies: an isotopic and REE study of Cambrian phosphorites. Chem. Geol. 175 (1–2), 29–48.
Shu, L.S., 2012. An analysis of principal features of tectonic evolution in South China Block. Geol. Bull. China 31 (7), 1035–1053 (in Chinese with English abstract).
Surya Prakash, L., Ray, D., Paropkari, A.L., Mudholkar, A.V., Satyanarayanan, M., Sreenivas, B., Chandrasekharam, D., Kota, D., Kamesh Raju, K.A., Kaisary, S., Balaram, V., Gurav, T., 2012. Distribution of REEs and yttrium among major geochemical phases of marine Fe–Mn-oxides: comparative study between hydrogenous and hydrothermal deposits. Chem. Geol. 312–313, 127–137.
Sverjensky, D.A., 1984. Europium redox equilibria in aqueous solution. Earth Planet. Sci. Lett. 67 (1), 70–78.
Takematsu, N., Sato, Y., Okabe, S., 1989. Factors controlling the chemical composition of marine manganese nodules and crusts: a review and synthesis. Mar. Chem. 26 (1), 41–56.
Tan, M.T., Lu, Z.X., Zhang, Y., 2009. Preliminary analysis on genesis of manganese in Datangpo Formation, western Hubei Province. Resour. Environ. Eng. 23 (2), 108–113 (in Chinese with English abstract).
Taylor, S.R., McLennan, S.M., 1985. The Continental Crust: Its Composition and Evolution. Scientific Publications, Blackwell, pp. 1–312.
Tribovillard, N., Algeo, T.J., Lyons, T., Riboulleau, A., 2006. Trace metals as paleoredox and paleoproductivity proxies: An update. Chem. Geol. 232 (1–2), 12–32.
Usui, A., Terashima, S., 1997. Deposition of hydrogenetic and hydrothermal manganese minerals in the Ogasawara (Bonin) Arc Area, Northwest Pacific. Mar. Georesour. Geotechnol. 15 (2), 127–154.
Wang, J., Liu, B.J., Pan, G.T., 2001. Neoproterozoic rifting history of south China significance to Rodinia break up. J. Miner. Petrol 21 (3), 135–145 (in Chinese with English abstract).
Wang, J., Zeng, Z.G., Chen, W.X., Wang, Z.J., Xiong, G.Q., Wang, X.H., 2006. The Neoproterozoic rift systems in southern China: new evidence for the sedimentary onlap and its initial age. Sediment. Geol. Tethyan Geol. 26 (4), 1–7 (in Chinese with English abstract).
Wang, P.M., Yu, J.H., Sun, T., Ling, H.F., Chen, P.R., Zhao, K.D., Chen, W.F., Liu, Q., 2012. Geochemistry and detrital zircon geochronology of Neoproterozoic sedimentary rocks in eastern Hunan Province and their tectonic significance. Acta Petrol. Sin. 28 (12), 3841–3857 (in Chinese with English abstract).
Wang, Y.G., Wang, L.X., Zhu, S.C., Xie, Z.Q., Chen, D.C., Zheng, S.F., Zhu, H., 1985. The Stratigraphy, Sedimentary Environment and Manganese-Forming Process of Datangpo Formation in Eastern Guizhou. Guizhou People Pub. House, Guiyang, pp. 1–92(in Chinese with English abstract).
Wang, Y.G., 1990. Old hot brine manganese deposits in a shallow-sea rift basin: an example from the Sinian manganese deposits in the Wuling mountain area. Sediment. Facies Palaeogeogr. 1, 38–45 (in Chinese with English abstract).

Wegorzewski, A.V., Kuhn, T., 2014. The influence of suboxic diagenesis on the formation of manganese nodules in the Clarion Clipperton nodule belt of the Pacific Ocean. Mar. Geol. 357, 123–138.

Wilde, P., Quinby-Hunt, M.S., Erdtmann, B.-D., 1996. The whole-rock cerium anomaly: a potential indicator of eustatic sea-level changes in shales of the anoxic facies. Sed. Geol. 101 (1–2), 43–53.

Wright, J., Schrader, H., Holser, W.T., 1987. Paleoredox variations in ancient oceans recorded by rare earth elements in fossil apatite. Geochim. Cosmochim. Acta 51, 631–644.

Xie, X.F., Qin, Y., Wen, G.G., Xie, X.Y., 2014. Relation between Datangpo Formation and manganese mineralization in Songtao manganese mining area of Tongren in Guizhou. Guizhou Geol. 31 (1), 32–37 (in Chinese with English abstract).

Xin, H., Jang, S.H., Yang, J.H., Wu, H.P., Pi, D.H., 2015. Rare earth element and Sr-Nd isotope geochemistry of phosphatic rocks in Neoproterozoic Ediacaran Doushantuo Formation in Zhangcunping section from western Hubei Province, South China. Palaeogeogr. Palaeoclimatol. Palaeoecol. 440, 712–724.

Xiong, Z., Li, T., Algeo, T., Chang, F., Yin, X., Xu, Z., 2012. Rare earth element geochemistry of laminated diatom mats from tropical West Pacific: evidence for more reducing bottomwaters and higher primary productivity during the Last Glacial Maximum. Chem. Geol. 296, 103–118.

Yang, R.D., Ouyang, Z.Y., Zhu, L.J., Wang, S.J., Jiang, L.J., Zhang, W.H., Gao, H., 2002. A new understanding of manganese carbonate deposits in early Sinian Datangpo stage. Acta Mineral. Sin. 22 (4), 329–334 (in Chinese with English abstract).

Yang, S.X., Lao, K.T., 2006. Mineralization model for the manganese deposits in northwestern Hunan: An example from Minle manganese deposit in Huayuan, Hunan. Sediment. Geol. Tethyan Geol. 26 (2), 72–80 (in Chinese with English abstract).

Ye, M.F., Li, X.H., Li, W.X., Liu, Y., Li, Z.X., 2007. SHRIMP zircon U-Pb geochronological and whole-rock geochemical evidence for an early Neoproterozoic Sibaoan magmatic arc along the southeastern margin of the Yangtze Block. Gondwana Res. 12 (1–2), 144–156.

Yin, C.Y., Wang, Y.G., Tang, F., Wan, Y.S., Wang, Z.Q., Gao, L.Z., Xing, Y.S., Liu, P.J., 2006. SHRIMPⅡ U-Pb zircon date from the Nanhuan Datangpo Formation in Songtao county, Guizhou province. Acta Geol. Sin. 80 (2), 273–278 (in Chinese with English abstract).

Zhang, F., 2014. The formation mechanism of Datangpo manganese ore deposits during Nanhua Period in South China and the paleo-redox conditions of Nanhua marine basin, Chinese Academy of Geological Sciences (master degree), pp. 1–121. (in Chinese with English abstract).

Zhang, F.F., Peng, Q.Y., Zhu, X.K., Yan, B., Li, J., Cheng, L., Si, X.H., 2013a. Fe istope characteristics of the Gucheng manganese ore deposits in Huibei province and its geological implication. Acta Geol. Sin. 87 (9), 1411–1418 (in Chinese with English abstract).

Zhang, F.F., Yan, B., Guo, Y.L., Zhu, X.K., Zhou, Q., Yang, D.Z., 2013b. Precipitation from of manganese ore deposits in Gucheng, Hubei province, and its paleoenvironment implication. Acta Geol. Sin. 87 (2), 245–258 (in Chinese with English abstract).

Zhang, F.F., Zhu, X.K., Gao, Z.F., Cheng, L., Peng, Q.Y., Yang, D.Z., 2013c. Implication of the precipitation mode of manganese and ultra-high $\delta^{34}S$ values of pyrite in Mn-carbonate of Xixibao Mn ore deposit in northeastern Guizhou province. Geol. Rev. 59 (2), 274–286 (in Chinese with English abstract).

Zhang, S.H., Jiang, G.Q., Han, Y.G., 2008. The age of the Nantuo Formation and Nantuo glaciation in South China. Terra Nova 20 (4), 289–294.

Zhao, D.X., 1990. Intraclastic structures and gravity flow sedimentation of rhodochrosite ore in Sinian Datangpo formation. Chin. J. Geol. 2, 149–158 (in chinese with English abstrace).

Zheng, G.X., Liu, X.F., 1987. The algae mineralization of the sedimentary dialogite deposits of Sinian and its diagenetic succession, Guizhou province. Guizhou Geol. 4 (3), 339–348 (in Chinese with English abstract).

Zhou, C.M., Tucker, R., Xiao, S.H., Peng, Z.X., Yuan, X.L., Chen, Z., 2004. New constraints on the ages of Neoproterozoic glaciations in south China. Geology 32 (5), 437–440.

Zhou, Q., Du, Y.S., Qin, Y., 2013. Ancient natural gas seepage sedimentary-type manganese metallogenic system and ore-forming model: a case study of Datangpo type manganese deposits formed in rift basin of Nanhua Period along Guizhou-Hunan-Chongqing border area. Miner. Deposits 32 (3), 457–466 (in Chinese with English abstrace).

Zhou, Q., Du, Y.S., Wang, J.S., Peng, J.Q., 2007a. Characteristics and significance of the cold seep carbonates from the Datangpoformation of the Nanhua series in the northeast Guizhou. Earth Sci. 32 (3), 339–346 (in Chinese with English abstract).

Zhou, Q., Du, Y.S., Yan, J.X., Zhang, M.Q., Yin, S.L., 2007b. Geological and geochemical characteristics of the cold seep carbonates in the early Nanhua system in Datangpo, Songtao, Guizhou province. Earth Sci. 32 (6), 845–852 (in Chinese with English abstract).

Zhu, B., Jang, S.Y., Yang, J.H., Pi, D.H., Ling, H.F., Chen, Y.Q., 2014. Rare earth element and Sr-Nd isotope geochemistry of phosphate nodules from the lower Cambrian Niutitang Formation, NW Hunan Province, Shouth China. Palaeogeogr. Palaeoclimatol. Palaeoecol. 398, 132–143.

Zhu, X.K., Peng, Q.Y., Zhang, R.B., An, Z.Z., Zhang, F.F., Yan, B., Li, J., Gao, Z.F., Qin, Y., Pan, W., 2013. Geological and geochemical characteristics of the Daotuo super-large manganese ore deposit at Songtao County in Guizhou province. Acta Geol. Sin. 87 (9), 1335–1348 (in Chinese with English abstract).